SPANWISE CORRELATION OF INSTANTANEOUS

WAKE STRUCTURE FOR FLAT PLATES:

THE EFFECT OF TRANSVERSE BODY VIBRATION

by

John J. TURNER, Lieutenant, USN

B.S. US Naval Academy
(1957)

Robert L. WARTERS, Lieutenant, USN

B.S. US Naval Academy
(1957)

SUBMITTED IN PARTIAL FULFILLMENT OF THE

REQUIREMENTS FOR THE DEGREE OF

NAVAL ENGINEER

AND THE DEGREE OF

MASTER OF SCIENCE IN NAVAL ARCHITECTURE

AND MARINE ENGINEERING

at the

MASSACHUSETTS INSTITUTE OF TECHNOLOGY

(MAY 1964)

SPANWISE CORRELATION OF INSTANTANEOUS

WAKE STRUCTURE FOR FLAT PLATES:

THE EFFECT OF TRANSVERSE BODY VIBRATION

by

John J. TURNER, Lieutenant, USN

B.S. US Naval Academy

(1957)

Robert L. WARTERS, Lieutenant, USN

B.S. US Naval Academy

(1957)

SUBMITTED IN PARTIAL FULFILLMENT OF THE

REQUIREMENTS FOR THE DEGREE OF

NAVAL ENGINEER

AND THE DEGREE OF

MASTER OF SCIENCE IN NAVAL ARCHITECTURE

AND MARINE ENGINEERING

at the

MASSACHUSETTS INSTITUTE OF TECHNOLOGY

(MAY 1964)

ABSTRACT

This thesis reports the results of an experimental investigation into the spanwise correlation of the fluctuating longitudinal velocity component in the early wake of a flat plate placed parallel to a uniform stream and allowed to vibrate about a vertical axis through the leading edge. The experimental program provides for the measurement of fluctuating total head signals at one fixed and one variable spanwise position on the wake center-line one body thickness downstream of the trailing edge. Analyzation of these signals gives the spanwise correlation of the wake structure expressed as a complex number and the power spectral density of the longitudinal velocity fluctuation along the span. In addition the mean local wake velocity is measured for each value of the ambient flow velocity.

Ambient velocities of 8, 11, and 14 fps and a single plate of $\frac{1}{4}$" thickness and 2" chord, were used for all the tests which were carried out in the $7\frac{1}{2}$" x 9" test section of an open-circuit water tunnel in the Hydrodynamics Laboratory at MIT.

An equation is developed which relates the vortex-induced forcing moment on the foil to the measured structure of the early wake. Using this model, forcing moment coefficients are evaluated as a function of a "self excitation" parameter consisting of the ratio of the mean transverse velocity of the trailing edge to the free stream velocity. The role of spanwise coherence of the wake is examined with respect to its effect on the coupling between body vibration and forcing moment.

Major Conclusion of this study is:

The increase in the forcing moment coefficient, m_{f_o}, accompanying an increase in the self excitation parameter is due to increasing correlation or coherency of the wake along the span rather than to increasing strength of the individual vortices being shed.

ACKNOWLEDGEMENTS

LIST OF SYMBOLS

$2b$	plate chord; 2 inches
f	frequency
$f(t)$	function of time
$F_1(n_1)$	Fourier transform of periodic signal of discrete frequency n_1
$F_2(n_2)$	Fourier transform of periodic signal of discrete frequency n_2
e	2.718
H	spanwise length of plate; in.
H_{tg}	fluctuating total head; ft. of water
$\overline{H}_{tg}$	mean total head; ft. of water
i	$\sqrt{-1}$
I_t	total moment of inertia; lbs-in-sec^2
K_t	total spring coefficient; lbs-in
m_f	average forcing moment coefficient; dimensionless
m_{f_o}	average amplitude of forcing moment coefficient; dimensionless
M	vortex induced forcing moment; lbs-in
n	discrete frequency
N	lift force on plate; lbs
p'	fluctuating static pressure; lbs/ft^2
$\overline{p}$	mean static pressure; lbs/ft^2
t	plate thickness; $\frac{1}{4}$ inches
t	time
u'	fluctuating longitudinal velocity component; fps
$\overline{u}$	mean local wake velocity; fps
V	mean ambient velocity outside the wake; fps
V_s	velocity of separation streamline; fps

v'	transverse fluctuating velocity; fps
$\bar{v}$	mean transverse velocity in the wake; fps
$V*$	$\dfrac{2b\omega\bar{\alpha}_o}{V}$, "self excitation" parameter; dimensionless
w'	spanwise fluctuating velocity in the wake; fps
$\bar{w}$	mean spanwise velocity in the wake; fps
x	longitudinal coordinate; origin at trailing edge
y	transverse coordinate; origin at trailing edge
z	spanwise coordinate; origin at mid-span
α	angular plate displacement; radians
$\bar{\alpha}_o$	RMS of vibrational amplitude; radians
γ	weight density of fluid; lbs/ft^3
Γ_o	vortex circulation; ft^2/sec
θ	phase angle of correlation
ϕ	phase angle between forcing moment and plate motion; radians
Φ_{AA}	cross power density; signal A, signal A
Φ_{BB}	cross power density; signal B, signal B
Φ_{AB}	cross power density; signal A, signal B

TABLE OF CONTENTS

LIST OF FIGURES

LIST OF TABLES

I   INTRODUCTION

A. Flow-Induced Vibrations

Structures subjected to a flow field may, under certain circumstances, experience flow-induced vibrations. These vibrations are undesirable and indeed may cause complete collapse of the structure due to fatigue induced by the vibrations.

Unstreamlined or "bluff" bodies in a flow field shed discrete vortices in the wake. The shedding of these vortices gives rise to periodic lift forces in a direction transverse to the flow direction. It has been shown in reference (2) that for bodies of finite thickness this vortex-induced lift force increases linearly with the transverse vibrational velocity, thus producing what may be called a "self-excited" vibration. The fluid mechanism involved in this feedback between motion and forcing force is unknown but may be expected to be due to an increase in the strength of the discrete vortices being shed and/or to an increase in the spanwise correlation of the vortices being shed.

B. Scope of the Investigation

The purpose of this investigation is to determine the cause of the amplitude dependence of the forcing moment so that engineers may devise steps to prevent the buildup of large amplitude vibrations.

2.

II EXPERIMENTAL EQUIPMENT

A. Water Tunnel

The experiment reported herein was carried out in the closed-jet, open circuit water tunnel of the Hydrodynamics Laboratory at MIT. The water tunnel is fully described in reference (1). Figure 1 shows the water tunnel test section. Pump number III (rated capacity 3000 G.P.M. at a head of 45 ft. and 1175 R.P.M.) was used.

Flow measurement was obtained using the tunnel contraction as a flow meter. Its calibration was checked and found to be the same as reported in reference (2).

B. Test Plate

The test plate used was plate D from reference (2), having the geometry shown in Figure 15. The plate was mounted vertically in the test section in such a way as to permit rotation about the center of its semi-circular leading edge. The plate is fabricated of aluminum.

C. Plate Motion Measurement

1. Strain Gages

Tatnall type C9-121-R2C strain gages were cemented to the torsion spring which restrains the plate motion and were waterproofed. The four gages form a wheatstone bridge which may be balanced by means of an external variable resistance. The bridge output voltage is proportional to the angle of plate rotation. See Appendix C of reference (2) for theory of calibration of the strain gage bridge.

2. Amplifier

A decade amplifier model 220-A made by Ballantine Laboratories Inc. was used to amplify the strain gage bridge output.

3.

3. Oscilloscope

An Eico model 460 DC-wide band oscilloscope was used for visual observation of the strain gage bridge output.

D. Total Head Fluctuation Measurements

1. Total Head Turbulence Gages

The gages for measuring the total head fluctuations (turbulence) are fully described in references (3 and 4). Figures 3 and 4, Appendix A, are photographs of the total head gages and Figure 15, Appendix A, is a drawing of the probes and test plate.

2. Electrometer Preamplifier

Two electrometers (one for each turbulence probe) were used to match the probe and amplifier impedences.

The electrometers are fully described in references (3 and 4). Figure 16 is a block diagram showing all electronic components.

3. Amplifiers

Two Dana model 2000 solid state, wideband, differential, low-level D.C. amplifiers with integral power supplies were used to amplify the turbulence probe signals. The amplifier has a flat response to $\pm$3db from DC to approximately 70 KC.

4. Oscilloscope

A Dumont type 333 dual beam oscilloscope was used for visual observations of the two turbulence probe signals.

5. Portable Tape Recorder

A Precision Instrument Co. portable tape recorder model PS 200 A was used to record the turbulence probe signals.

6. Endless Loop Tape Recorder

A Sanborn model 2000 endless loop tape recorder was used to give a continuous input of the turbulence probe signals into the wave analysis system.

7. Wave Analysis System

To analyze the turbulence probe signals, a Technical Products Co. TP 625 Wave Analyzer System was used. This system consists of the following:

a. One TP 626 Oscillator

This oscillator produces an output frequency which is continuously variable from 97 KC to 122 KC over three different frequency bands: 97.0 KC - 97.25 KC; 97.0 KC - 99.5 KC; and 97.0 KC - 122.0 KC. The oscillator output is used to modulate the signal to be analyzed in the TP 627 analyzers.

b. Two TP 627 Analyzers

These analyzers determine the frequency and amplitude of the individual components of a complex wave within the frequency range of 2-25,000 cycles. The results are measured in percent of total signal.

These analyzers are equipped with two matched TP-218 type filters as required for operation in conjunction with a TP-645 Multiplier.

c. One TP-645 Multiplier

This multiplier, when used in conjunction with the other components of the system, gives the cross power spectrum of two complex waves within the frequency range of 2-25,000 cycles.

III THEORY

A. Forcing Moment Coefficient

In reference (2) Noutsopoulos develops the equation of motion of a single degree of freedom plate spring system vibrating about an axis through the leading edge of the plate. The motion is caused by a forcing moment resulting from flow separation at the trailing edge of the plate. Assuming two-dimensional motion, the equation of motion of the plate may be written

$$I_t \ddot{\alpha} + C_t \dot{\alpha} + K_t \alpha = M$$

where I_t = the total moment of inertia

C_t = the total damping coefficient

K_t = the total stiffness of the system

and α = the angular plate displacement in radians $\alpha = \alpha_0 e^{i\omega t}$.

From purely dimensional considerations, the simplest form of the forcing moment can be written

$$M = m_f \tfrac{1}{2} \rho H (2b)^2 V^2$$

where m_f is the spanwise average forcing moment coefficient, H is the span and V the ambient fluid velocity. When the forcing moment is periodic as in the case of excitation by vortex shedding, the moment coefficient is conveniently written in complex form as

$$m_f = m_{f_0} e^{i(wt + \phi)}$$

where w = angular frequency of vortex shedding from one side of the plate in cps

ϕ = phase angle tetween the spanwise average forcing moment and the motion α.

t = time in seconds.

The moment on the plate may also be written in terms of a lift force and an appropriate moment arm where the lift force is a function of the circulation which is a measure of the vortex strength.

Therefore

$$M \sim 2bN$$

where 2b is the chord length and

N is the lift force.

The lift force may be written as

$$N = \rho V \Gamma H$$

where Γ is the circulation on the plate and is a function of position along the span and time such that:

$$N = \rho V \int_0^H \Gamma (z,t)dz .$$

If the circulation is considered to be a periodic function then

$$\Gamma (z,t) = \Gamma_0(z) e^{i(wt + \phi + \theta(z))}$$

with $\theta(z)$ being the phase angle of the circulation at some position, z, along the span, measured with respect to the value, ϕ, at midspan of the plate so that

$$N = \rho V e^{i(wt + \phi)} \left[\int_0^H \Gamma_0(z)\cos \theta \, dz + i \int_0^H \Gamma_0(z) \sin \theta \, dz \right]$$

Assuming application of the lift force at the trailing edge the moment on the plate may be written as

$$M = 2bN$$

$$M = 2\rho Vbe^{i(wt + \phi)} \left[\int_0^H \Gamma_0(z)\cos \theta \, dz + i \int_0^H \Gamma_0(z)\sin \theta \, dz \right].$$

It is now assumed that

$$\Gamma_0 \sim \frac{\overline{(u'_B)^2}}{f}$$

where Γ_0 = circulation in the vortex

u'_B = the longitudinal fluctuating velocity component as measured by probe B

and f = vortex shedding frequency.

From reference (4)

$$\Gamma_0 \sim \frac{\overline{V_s^2}}{f}$$

where V_s = the velocity of the separation streamline. So that the assumption here is that

$$u'_B \sim V_s$$

Substituting for $\Gamma_0(z)$ the moment may be written

$$M \sim \rho V b e^{i(wt + \phi)} \left[\int_0^H \frac{\overline{u'^2_B}}{f} \cos \theta \, dz + i \int_0^H \frac{\overline{u'^2_B}}{f} \sin \theta \, dz \right]$$

Now assuming the moment coefficient to be a real quantity and equating the two expressions for moment we have

$$\overline{m}_{f_0} \sim \left[fbHV \right]^{-1} \left[\int_0^H \overline{u'^2_B} \cos \theta \, dz \right]$$

and

$$\int_0^H \overline{u'^2_B} \sin \theta \, dz = 0$$

Here the assumption is that the wake is symmetrical behind the plate, so that the integral of an odd function is zero. Therefore, the forcing moment coefficient is proportional to the integral

$$\int_0^H \overline{u_B'^2} \cos\theta \, dz$$

where $\overline{u_B'^2}$ is the longitudinal fluctuating velocity component measured by the traversing turbulence probe (probe B).

B. Turbulence Probes

Reference (4) describes the development and theory of the total head tube in detail. Briefly the following is a resume of the theoretical considerations involved in the measurements.

In general the instantaneous response of a total head tube may be written

$$H_{tg} = \frac{\overline{p}}{\delta} + \frac{p'}{\gamma} + \frac{(\overline{u} + u')^2}{2g} + \frac{(\overline{v} + v')^2}{2g} + \frac{(\overline{w} + w')^2}{2g}$$

where p is the pressure and u, v, and w are the velocity components in the coordinate direction. The barred quantities are mean values and the primed symbols are fluctuating values.

From the geometry of the probe, it is a good assumption that the turbulence probe is much more sensitive to the velocity components parallel to the mean flow than to those which are perpendicular to the mean flow (i.e., the terms $v'^2/2g$ and $w'^2/2g$ are neglected). Also low frequency response of the piezoelectric crystal makes the turbulence probe insensitive to mean quantities.

Therefore the instantaneous total head response becomes with these assumptions:

$$H_{tg} = \frac{p'}{\gamma} + \frac{2\overline{u}u'}{2g} + \frac{u'^2}{2g}$$

The D.C. portion of this signal (the time average of the fluctuation) is given by:

$$\overline{H_{tg}} = \frac{\overline{u'^2}}{2g}$$

The D.C. level is removed by a filter so that

$$H_{tg} - \overline{H_{tg}} \;=\; \frac{p'}{\gamma} + \frac{\overline{uu'}}{g} + \frac{u'^2}{2g} - \frac{\overline{u'^2}}{2g}$$

An important assumption at this stage is that all terms on the right hand side of the equation can be ignored with respect to $\overline{u}u'/g$, whereupon

$$H_{tg} - \overline{H_{tg}} \;=\; \frac{\overline{u}u'}{g}$$

and the electrical signal as measured by the turbulence probe is proportional to the product of $\overline{u}u'$, the product of the mean longitudinal wake velocity and the longitudinal fluctuating velocity component.

C. The Wave Analysis System

The two electrical signals measured by the two turbulence probes located in the wake of the plate and positioned along the span were analyzed by the wave analysis system.

In general the wave analysis system accepts one or two periodic or random signals as inputs and provides as output the power density of either signal and the cross power density expressed as a complex number. The power density is a representation of the amount of power in the input signal contained in a given bandwidth. The cross power density is a measure of the power (contained in a frequency bandwidth) common to the two input signals.

If the probe signals were harmonic they could be written as functions of time as $f_A(t)$ and $f_B(t)$ and their transforms as $F_A(n_1)$ and $F_B(n_2)$. If $F_A(n_1)$ is multiplied by $\overline{F_B}(n_2)$, the complex conjugate of $F_B(n_2)$, and the product is averaged in time, only products of common frequencies remain so that $\oint_{AB}^{(n)} = \overline{F_A(n)\overline{F_B}(n)} \equiv$ cross power density. $\oint_{AB}^{(n)}$ may also be written

$$\Phi_{AB}(n) = \sqrt{PSD_A} \ \sqrt{PSD_B}$$

This can be shown since

$$F_1(n) = \frac{1}{T_1} \int_{-\frac{T_1}{2}}^{\frac{T_1}{2}} f_1(t) \ e^{-in\omega_1 t} \ dt$$

$$F_2(n) = \frac{1}{T_1} \int_{-\frac{T_1}{2}}^{\frac{T_1}{2}} f_2(t) \ e^{-in\omega_1 t} \ dt$$

and

$$\frac{1}{T_1} \int_{-\frac{T_1}{2}}^{\frac{T_1}{2}} f_1(t)f_2(t+\tau)dt = \frac{1}{T_1} \int_{-\frac{T_1}{2}}^{\frac{T_1}{2}} f_1(t)dt \sum_{n=-\infty}^{\infty} F_2(n)e^{in\omega_1(t+\tau)}$$

$$= \sum_{n=-\infty}^{\infty} F_2(n)e^{in\omega_1\tau} \frac{1}{T_1} \int_{-\frac{T_1}{2}}^{\frac{T_1}{2}} f_1(t)e^{in\omega_1 t} \ dt$$

therefore

$$\frac{1}{T_1} \int_{-\frac{T_1}{2}}^{\frac{T_1}{2}} f_1(t)f_2(t+\tau)dt = \sum_{n=-\infty}^{\infty} \left[\overline{F_1}(n)F_2(n) \right] e^{in\omega_1\tau}$$

and

$$\overline{F_1}(n)F_2(n) = \frac{1}{T_1} \int_{-\frac{T_1}{2}}^{\frac{T_1}{2}} e^{-in\omega_1\tau} \ d\tau \ \frac{1}{T_1} \int_{-\frac{T_1}{2}}^{\frac{T_1}{2}} f_1(t)f_2(t+\tau)dt$$

but

$$\Phi_{AB} \equiv \frac{1}{T_1} \int_{-T_{\frac{1}{2}}}^{T_{\frac{1}{2}}} e^{-in\omega_1 \tau} d\tau \; \frac{1}{T_1} \int_{-T_{\frac{1}{2}}}^{T_{\frac{1}{2}}} f_1(t)f_2(t+\tau)dt$$

and since machine operation gives

$$F_1(n) = \sqrt{PSD_A}$$

$$\overline{F_2}(n) = \sqrt{PSD_B}$$

then

$$\Phi_{AB} = \sqrt{PSD_A} \; \sqrt{PSD_B}$$

The TP 625 wave analyzer system accomplishes this by passing the random

input signals $f_A(t)$ and $f_B(t)$ through a set of amplitude and phase matched

band pass filters before multiplication. In order to preserve the phase

angle Θ between the two input signals, two modes of operation of the

multiplier yield the real and imaginary parts of a complex number called

the co-spectrum and the quad-spectrum respectively so that

$$\left| \Phi_{AB} \right| = \left[(\text{co-spectrum})^2 + (\text{quad-spectrum})^2 \right]^{\frac{1}{2}}$$

and

$$\Theta = \tan^{-1} \frac{\text{quad-spectrum}}{\text{co-spectrum}}$$

For random signals these quantities have the units of power density or power

divided by the filter band-pass at the center frequency of the filter.

Now if it is assumed that the signal from probe B is correlated

(i.e., similar) with the signal from probe A, the fixed probe, we can write

$$u_A' = K(z) u_B'$$

where $K(z)$ represents the proportionality between the signals as a function

of their spanwise separation. As noticed previously the output of the
probes are $u'\bar{u}$ so that $\left|\bar{\Phi}_{AB}\right| \sim \overline{u'_A u'_B \bar{u}^2}$. Note that it is tacitly
assumed that $\bar{u}_A = \bar{u}_B$. Therefore

$$\left|\bar{\Phi}_{AB}\right|^2 \sim \overline{u'_A u'_B \bar{u}^2} \cdot \overline{u'_A u'_B \bar{u}^2}$$

and if we divide by $\left|\bar{\Phi}_{AA}\right|\bar{u}^2$ we have

$$\frac{\left|\bar{\Phi}_{AB}\right|^2}{\Phi_{AA}\,\bar{u}^2} \sim \frac{\overline{u'_A u'_B \bar{u}^2} \cdot \overline{u'_A u'_B \bar{u}^2}}{\overline{u'_A u'_A \bar{u}^2} \cdot \bar{u}^2}$$

Substituting for u'_A

$$\frac{\left|\bar{\Phi}_{AB}\right|^2}{\Phi_{AA}\,\bar{u}^2} \sim \frac{\overline{K(z)u'^2_B} \cdot \overline{K(z)u'^2_B}}{\overline{K(z)^2\,u'^2_B}}$$

$$\sim \overline{u'^2_B}$$

Since wave analyzer operation gives

$$\Phi_{AA} = PSD_A$$

then

$$\frac{\left|\bar{\Phi}_{AB}\right|^2}{PSD_A\,\bar{u}^2} \sim \overline{u'^2_B}$$

and referring to the discussion of the forcing moment coefficient where

$$m_{f_o} \sim \left[fbHV \right]^{-1} \int_0^H \overline{u_B'^2} \cos \theta \, dz$$

This suggests a method of evaluating the integral. $\left| \Phi_{AB} \right|$ and PSD_A values are available as outputs of the wave analysis system and values of $\overline{u}$ are easily measured in the tunnel. Values of θ are available as shown from

$$\theta = \tan^{-1} \frac{\text{quad-spectrum}}{\text{co-spectrum}} \ .$$

IV PROCEDURE

A. Total Head Turbulence Probe Calibration

The total head turbulence probes, electrometer preamplifiers, D.C. filters, and the turbulence probe signal amplifiers were calibrated as assembled units. The two system outputs were adjusted by changing the amplifier gain on one system so that the output of the two systems were equal for identical inputs. Figures 5 and 6, Appendix A, show the amplified turbulence probe signals when the probes were subjected to a step impulse. See reference (2) for calibration details.

B. Tunnel Measurements

The fixed turbulence probe was initially positioned in the tunnel at $y/t = 0$ and $x/t = 1$. See Figure 15, Appendix A for description of coordinate system. Alignment of the traversing turbulence probe (probe B) with respect to the fixed probe (probe A) is assured by the method of attachment of the two probes and the proper positioning of the traversing probe seal at the bottom of the test section. Measurements were taken with the plate free to vibrate at ambient velocities of 8, 11, and 14 fps, and clamped in a fixed position at an ambient velocity of 14 fps. The velocities were obtained from the contraction meter as described in reference (2). Mean wake velocities were measured as described in reference(3). While maintaining a constant ambient velocity by operation of the inlet and foot valves, the turbulence probe signals, plate vibration signal and a marker signal were recorded on four channels of the protable tape recorder for each spanwise position (z/t) of the traversing probe. Prior to and during the actual recording, the signals were monitored on oscilloscopes to insure that the proper signals were recorded. The pressure in the tunnel was maintained

at the same value by operation of the foot valve and was kept sufficiently high (3 psi) to prevent cavitation.

C. Data Analysis

The recorded signals were analyzed with the Technical Products Company TP 625 Wave Analyzer System. Each run consisted of a recording of the four signals (two fluctuating total heads, plate vibrational amplitude, marker) at a particular z/t and velocity. For each run the probe signals were rerecorded on a Sanborn-Ampex 2000 continuous loop tape recorder for con- tinuous play back into the wave analyzer system. Prior to each analyzation, the wave analyzer system was carefully calibrated with a 100 cps, 0.46 volt peak to peak oscillator signal. The gains of the two wave analyzers were set the same and the oscillator (TP 626) output indicator was adjusted with a reference oscillator to ensure accurate frequency readings. The gains of the two analyzers TP 627 were matched and the Power Spectral Density set- tings of the multiplier TP 645 were adjusted to give the same output for identical inputs. In addition the phasing between the identical input signals was zeroed using the phase zero dial. Calibration in this manner ensures that the relative power levels in the signals are preserved in the output, and that zero phase angle is indicated for identical input signals. The output of the wave analysis system is in volts and is only a relative measure. A 50 cps. band width filter and a long averaging time (2 seconds) were chosen for the analyzation. The filter and 2 second averaging time were selected to give smooth curves from which data points could be accurately determined.

For z/t = 1 and 9 at each velocity, the power spectrum density for each signal and the co-spectrum and quad-spectrum were obtained. For the remaining valves of z/t, the power spectrum density of "B" (the movable

turbulence probe), co-spectrum and quad-spectrum were obtained.

The horizontal scale of the x-y plotter was adjusted so that a full sweep covered from 50 to 200 cps. The vertical scale of the x-y plotter was set to 1 volt per inch. Also for $z/t = 9$ at each velocity, the power spectrum density "B" was obtained using a 1 cps band width filter and an averaging time of 0.2 seconds to indicate the exact frequency of the energy in the wake. Similarly for the plate motion signal, a spectrum was obtained to pinpoint the frequency of plate vibration.

V PRESENTATION AND DISCUSSION OF RESULTS

The outputs of the Wave Analyzer system are the power density spectrum of a single signal, the co-spectrum, and the quad-spectrum of the two signals taken jointly. These are presented for each run as Appendix C.

For analyzation purposes, frequencies of 75 cps for runs with the test plate free to vibrate and 105 cps for runs with the test plate fixed were chosen. These frequencies were selected because they were the respective points of peak power as indicated by the plots of power spectrum density (PSD) and hence represent the frequency of vortex shedding. This reason for frequency selection is reinforced by the PSD of the vibrating plate signals which also has its peak power at 75 cps. See the power spectrum density for vibrating plate signals, runs 11, 16, and 21, Appendix C.

Power density spectra were obtained from the wave analyzer system with narrow filter settings as well as with wide filter settings for runs 6, 11, 16, and 21. These narrow filter power density spectra show more clearly the exact frequency of peak power than do the power density spectra made with wide filter settings.

Table 1, Appendix B, lists the values of PSD, co-spectra and quad-spectra used in the following analysis.

Power density spectra for probe A (fixed probe) are shown in Appendix C for runs 1, 6, 7, 11, 12, 16, 17, and 21. These are all runs with probe separation $(z/t) = 1$ and 9. It can be seen that for each velocity PSD_A is the same for all probe separations z/t. This indicates that at small probe separation, one probe does not affect the signal of the other probe and that the signal from the turbulence probe A is stationary.

The power density for the fixed probe A increases in magnitude at the plate vibration frequency with an increase in ambient velocity. However

the power densities for the fixed plate (runs 1 through 6 of Appendix C, ambient velocity - 14 ft/sec) are higher than are the power densities for the vibrating plate runs with the same ambient velocity as the fixed plate runs (see runs 17 through 21 of Appendix C for vibrating plate runs with an ambient velocity of 14 ft/sec). Thus power density is not a function of ambient velocity alone.

If one computes the self excitation parameter of reference (2), $V* = \frac{2b\omega\bar{\alpha}_0}{V}$, for each run made in this study and compares Φ_{AA} and $V*$, it can be seen that Φ_{AA} decreases as the self excitation parameter $V*$ increases. $V*$ is the ratio of the transverse velocity of the trailing edge of the test plate to the ambient water velocity.

It has been shown in Section III that the power density spectrum, Φ_{AA}, is proportional to $(u_A'\bar{u})^2$. Thus $\Phi_{AA}/\bar{u}^2$ is proportional to $(u_A')^2$. The quantity, $(u')^2/f$, may be considered a measure of the strength of the individual vorticies. Thus $\Phi_{AA}/\bar{u}^2 f$ is proportional to the strength of vortices being shed. Figure 19 shows the strength of the vortices $\Phi_{AA}/\bar{u}^2 f$ being shed plotted vs. the self excitation parameter $V*$. Figure 19 shows that the vortex strength drops off rapidly with an increase in the self excitation parameter $V*$. Thus the increase in forcing moment co-efficient m_{f_0} with an increase in the self excitation parameter $V*$ cannot be explained by an increase in the strength of the vortices being shed.

For the case of the fixed plate ($V* = 0$) it appears that the values of vortex strength and coherency may vary with the ambient velocity.

The power density spectra for the signal from probe B at small separations (runs 1, 7, 12, and 17 of Appendix C) are essentially the same as the power density spectra for the signals from probe A.

As shown in Section III:

$$\left|\Phi_{AB}\right| = \left[(\text{co-spectrum})^2 + (\text{quad-spectrum})^2\right]^{\frac{1}{2}}$$

$$\theta = \tan^{-1}\frac{\text{quad-spectrum}}{\text{co-spectrum}}$$

Table 1 lists the values of $\left|\Phi_{AB}\right|$ and θ for all runs. As explained in Section IV, Procedure, the wave analyzer system was adjusted so that the outputs were all relative to the 100 cycle sine wave calibration signal.

The Technical Products Company wave analyzer system when in the power spectrum density mode of operation, multiplies the input signal by itself and in effect becomes a squarer. Time averaging then eliminates all products except those of common frequencies. Thus the power spectrum density of signal A $= \Phi_{AA} \sim \overline{(u_A'\overline{u})^2}$; likewise $\Phi_{BB} \sim \overline{(u_B'\overline{u})^2}$. When the wave analyzer system is used to obtain the cross power spectrum density the two input signals are again multiplied and time averaged.

When interpreting the machine output we must remember that all Φ's are averages over a finite bandwidth. Thus when we look at Φ_{AA} or Φ_{BB} with the filter centered at frequency n_o, $F_A(n_o)$ or $F_B(n_o)$ may be zero yet Φ_{AA} or Φ_{BB} can be non zero due to contributions at other frequencies within the filter pass-band. When looking at Φ_{AB} we are most interested in its value at the vortex shedding frequency. If this frequency is only slightly different at the locations of probes A and B, and the random turbulent background at surrounding frequencies is negligibly small, Φ_{AB} can be zero and yet Φ_{AA} and Φ_{BB} would be non-zero!

Since $\left|\Phi_{AB}\right| \sim \overline{(u_A'u_B'\overline{u}^2)}$, $\Phi_{AA} \sim \overline{(u_A'\overline{u})^2}$ and $\Phi_{BB} \sim \overline{(u_B'\overline{u})^2}$, then $\left|\Phi_{AB}\right| \sim \left[\Phi_{AA}\right]^{\frac{1}{2}}\left[\Phi_{BB}\right]^{\frac{1}{2}}$ where u_A' and u_B' have the same frequencies. Therefore $\left|\Phi_{AB}\right|$ is a measure of overall signal strength as well as a measure of the similarity of the two signal amplitudes. To eliminate the

effect of overall signal strength all values of $\left|\Phi_{AB}\right|$ for each velocity can be normalized by their respective Φ_{AA} values (for each velocity Φ_{AA} is stationary as shown in Appendix C).

Therefore: $\Phi^* \equiv \left|\Phi_{AB}\right| / \Phi_{AA}$ and is only a measure of the similarity of signal A and signal B. Values of Φ^* are tabulated in Table 1, Appendix B. Figure 17 is a plot of Φ^* vs. z/t for different values of the dimensionless self excitation parameter $V* = \dfrac{2b\omega\bar{a}_o}{V}$. Figure 18 is a plot of θ vs. z/t for different values of V*.

Vibrating plate runs at an ambient velocity of 14 fps were repeated after a two week interval to investigate the reproducability of the experimental data. Figure 21 compares values of Φ^* and θ vs. z/t. It can be seen from this figure that the cross power spectra compare very favorably, but a phase angle variation is to be expected.

From Figure 17 it can be seen that the correlation of the turbulence probe signals for vibrating plate runs decreases as probe separation increases which is what one would expect. Figure 17 also shows that the normalized cross power density increases for vibrating plate runs with an increase in the self excitation parameter V*.

Figure 19 shows that the normalized cross power density Φ^* increases as the self excitation parameter V* increases.

Figure 18 shows that for z/t < 5 for vibrating plate runs there is a gradual increase in θ as z/t increases, but there is no significant change in θ for an increase in the self excitation parameter V*. For probe separation z/t > 5 for vibrating plate runs θ increases with an increase in z/t and decreases as the self excitation parameter V* increases.

Figures 17, 18, and 19 show that the shedding of the vortices becomes more correlated and more in phase as the self excitation parameter V* increases.

For the self excitation parameter V* = 0 (fixed plate) with a velocity of 14 ft/sec, Figure 17 shows Φ^* to decrease to near zero at z/t $\approx$ 7 and Φ^* to increase for values of z/t > 7. For V* = 0 Figure 18 shows θ to increase gradually for values of z/t < 6 and θ to increase rapidly to values > 180° for values of z/t > 6. This indicates that for V* = 0 there may be a spanwise cellular structure with alternate cells 180° out of phase. Assuming symmetry the wavelength of the cell would be 14 body thicknesses. Roshko (6) reports a 18 diameter wavelength for measurements behind a circular cylinder at a body Reynolds number of 80.

As shown in Section III:

$$m_{f_o} \sim (bHf\overline{Vu}_B{}^2)^{-1} \int_0^H \frac{|\Phi_{AB}|^2}{\Phi_{AA}} \cos\theta \, dz$$

Values of $(|\Phi_{AB}| \cos\theta)/(\Phi_{AA})$ were plotted vs. z/t and integrated from z/t = 1 to z/t = 9. It was assumed that the value of this integral is proportional to the integral evaluated over the entire plate span.

m_{f_o} was calculated by

$$m_{f_o} \sim (fV\overline{u}^2)^{-1} \int_1^9 \frac{|\Phi_{AB}|^2}{\Phi_{AA}} \cos\theta \, d(z/t)$$

These values of m_{f_o} for the vibrating plate runs are plotted vs. V* in Figure 20, Appendix B. The dotted line in Figure 20 is a plot of m_{f_o} vs. V* as determined from reference (2). It can be seen that these two plots of m_{f_o} are in qualitative agreement. In an effort to determine any predominence of either $|\Phi_{AB}|^2/\Phi_{AA}$ or θ in the integrand of the equation used to determine m_{f_o} (i.e., is the amplitude coherence or the phase coherence, the predominant factor in

$$m_{f_o} \sim (f V \bar{u}^2)^{-1} \int \frac{\left|\Phi_{AB}\right|^2}{\Phi_{AA}} \cos \vartheta \, d(z/t)? \,)$$ it was assumed that $\cos \vartheta$ was

constant, hence

$$m_{f_o} \sim (f V \bar{u}^2)^{-1} \int_{1}^{z/t=9} \frac{\left|\Phi_{AB}\right|^2}{\Phi_{AA}} \, d(z/t)$$

The resulting m_{f_o} plotted vs. V* is shown in Figure 20.

Next it was assumed that $(\left|\Phi_{AB}\right|^2)/(\Phi_{AA})$ was constant, hence

$$m_{f_o} \sim (f V \bar{u}^2)^{-1} \int_{1}^{z/t=9} \cos \vartheta \, d(z/t)$$

The resulting m_{f_o} plotted vs. V* is shown in Figure 20.

The conclusion drawn from this fugure is that it is impossible to

determine the predominate factor in

$$m_{f_o} \sim (f V \bar{u}^2)^{-1} \int \frac{\Phi_{AB}^2}{\Phi_{AA}} \cos \vartheta \, d(z/t)$$

Undoubtedly both $(\left|\Phi_{AB}\right|^2)/(\Phi_{AA})$ and $\cos \vartheta$ are important. Indeed it may

be said that amplitude correlation and phase correlation have no significance

unless presented together. Phase correlation has no significance unless

there is some amplitude correlation and vice versa.

The calculated values of m_{f_o} for the fixed plate runs assuming that

the integrals evaluated from $z/t = 1$ to $z/t = 9$ were proportional to the

same integrals evaluated over the entire plate were not considered valid.

However, by extrapolation of the integrand over the entire length, assuming

a cellular structure with alternate cells 180° out of phase, values of m_{f_o}

obtained are in qualitative agreement with reference (2).

The co-spectrum of the vibrating plate runs, runs 7 - 21, Appendix C,

show that some correlation exists at 140 cycles. This correlation was not

investigated, but it could be the correlation of the first harmonic of the vortex shedding frequency. The vibrating plate spectra for runs 16, 21 Appendix C, show power at about 140 cycles, and this could explain the correlation at 140 cycles.

VI   SUMMARY AND CONCLUSIONS

Spanwise cross correlations of the longitudinal turbulent velocity component in the early wake of a flat plate were measured in water under conditions of flow-induced torsional vibration of the plate in order to ascertain the nature of the known dependence of the forcing moment upon the ratio of vibratory plate velocity to free-stream fluid velocity.

The following conclusions are drawn:

1.   The increase in the forcing moment coefficient m_{f_o} with the self excitation parameter $V*$ is due to an improvement in correlation or coherency of the wake along the span rather than to increasing strength of the individual vortices being shed.

2.   The forcing moment coefficient can be expressed in the form

$$\overline{m_{f_o}} \sim (fbH V \overline{u^2})^{-1} \int_0^H \frac{\left| \Phi_{AB} \right|^2}{\Phi_{AA}} \cos \theta \, dz$$

3.   Both the absolute magnitude of the cross power density Φ^* and its phase angle θ are important in explaining the relationship between the forcing moment coefficient m_{f_o} and the self excitation parameter. Spanwise variations in phase angle are shown to be reduced with increasing $V*$ and coherence of vortex strength at the vibrational frequency is increased.

4.   Measurements of the spanwise wake structure under conditions in which plate vibrations are prevented are consistent with a cellular structure with a phase shift of 180° between alternate cells.

5.   In order to minimize self-induced vibration, engineers should design structures in such a way as to eliminate wake coherency. This

might be accomplished by a random spanwise variation of trailing edge geometry, or by attaching to the trailing edge short independent sections which are free to rotate about the trailing edge.

VII <u>RECOMMENDATIONS</u>

1. In the co-spectrum of probe B some indication of correlation was observed at 140 cps. It is recommended that this be investigated.

2. It is recommended that measurements such as taken in this study be taken so as to include observations of the wake along the entire span. This will necessitate a new turbulence probe supporting mechanism.

3. It is recommended that a 5, 10, or 20 cycle bandwidth filter be obtained for the Technical Products Wave Analyzer System. These more narrow filters will permit a more accurate determination of the frequencies of peak power in both the power spectrums and the cross power spectrums. The available one cycle filter proved to be too narrow for the random signal involved.

VIII REFERENCES

1. Toebes, G. H., F. E. Perkins, and P. S. Eagleson; "Design of a Closed Jet, Open Circuit Water Tunnel for the Study of Wake Mechanics," MIT, T.N. 3, Hydro. Lab., April 1958.

2. Noutsopoulos, G. K.; "Flow-Induced Vibrations of Flat Plates: Moment Coefficients and Wake Structure," Sc.D. Thesis, MIT Department of Civil Engineering, September 1962.

3. Eagleson, P. S., C. J. Huval, and F. E. Perkins; "Turbulence in the Early Wake of a Fixed Flat Plate," MIT Hydro. Lab., T.R. 46, February 1961.

4. Perkins, F. E., and P. S. Eagleson; "The Development of a Total Head Tube for High Frequency Pressure Fluctuations in Water," MIT Hydro. Lab., T.N. 5, July 1959.

5. Technical Products Company, Instruction Manual for TP 625 Wave Analyzer System.

6. Roshko, A.; "On the Development of Turbulent Wakes from Vortex Streets," NACA Rep. 1191, 1954.

APPENDIX A

ILLUSTRATIONS

TITLES OF PICTURES ON THE FOLLOWING PAGE

Figure 1:   Water tunnel test section showing electrometers, amplifiers, DC filters, and strain gage controls.

Figure 2:   Left: Sanborn 2000 tape recorder.

                Center bottom: Precision Instrument Company portable tape recorder.

                Right: Technical Products wave analyzer system.

Figure 3:   Probes and supporting structure.

Figure 4:   Probes and supporting structure.

FIG.
2

FIG.
1
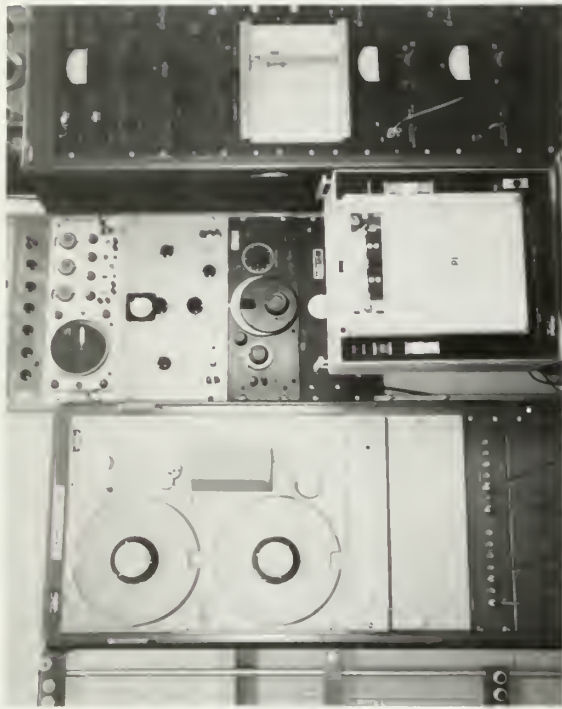
SEE
PREVIOUS
PAGE
FOR
PICTURE
TITLES

FIG.
4

FIG.
3
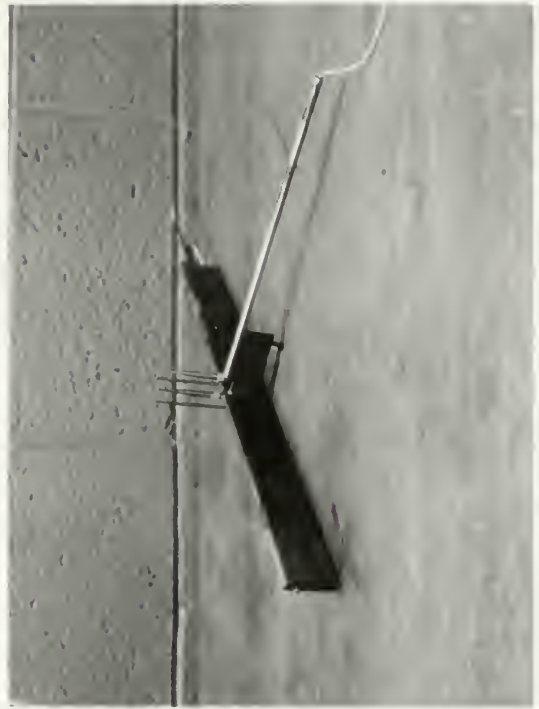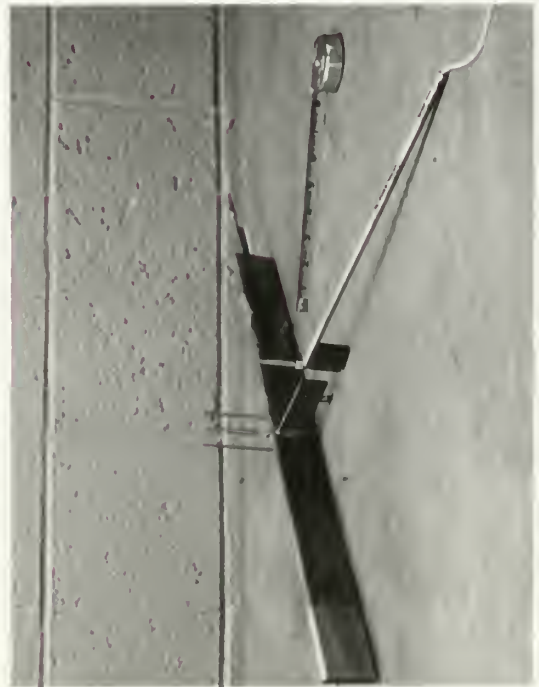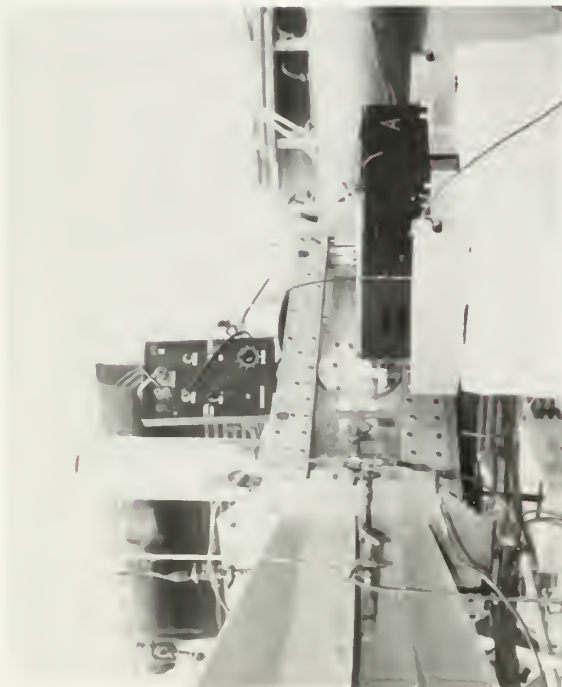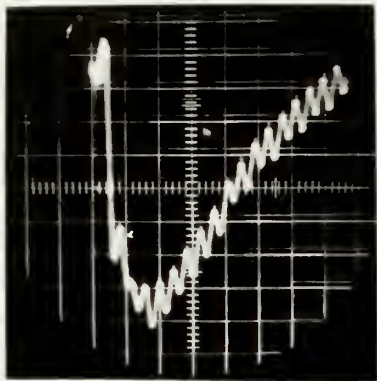
FIG. 5
PROBE A SIGNAL
CALIBRATION
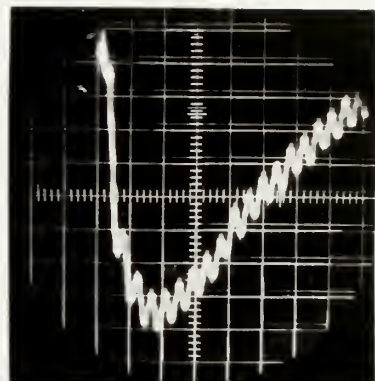
FIG. 6
PROBE B SIGNAL
CALIBRATION
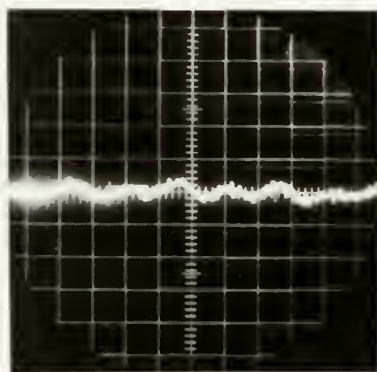
FIG. 7
PROBE A SIGNAL
VEL.= 0 FT./SEC.
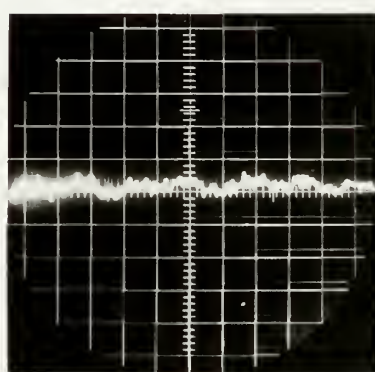
FIG. 8
PROBE B SIGNAL
VEL.= 0 FT./SEC.
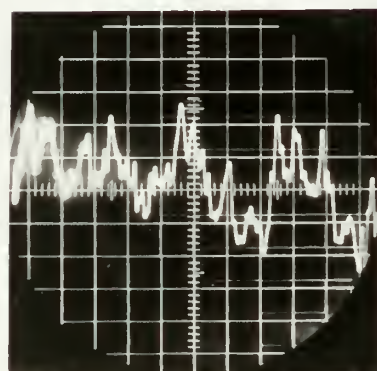
FIG. 9
PROBE A SIGNAL
VEL.= 11 FT./SEC.
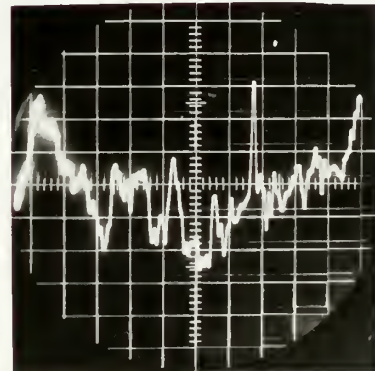
FIG. 10
PROBE B SIGNAL
VEL.= 11 FT./SEC.
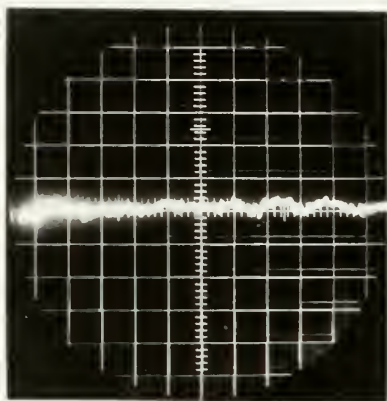
FIG. 11
PLATE SIGNAL
VEL.= 0 FT./SEC.
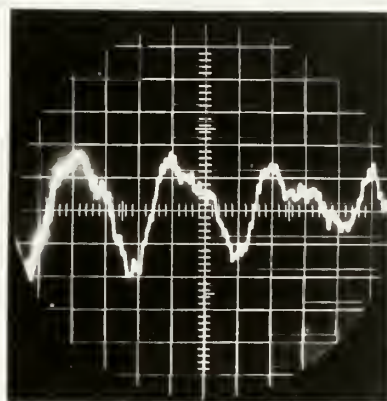
FIG. 12
PLATE SIGNAL
VEL.= 8 FT./SEC.
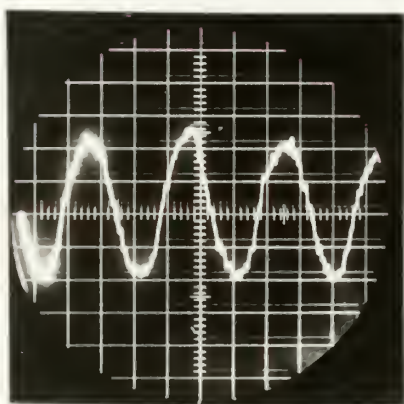
FIG. 13
PLATE SIGNAL
VEL.= 11 FT./SEC.
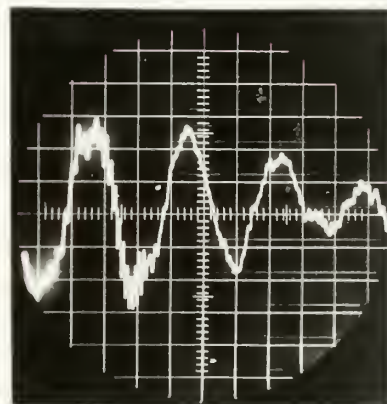
FIG. 14
PLATE SIGNAL
VEL.= 14 FT./SEC.
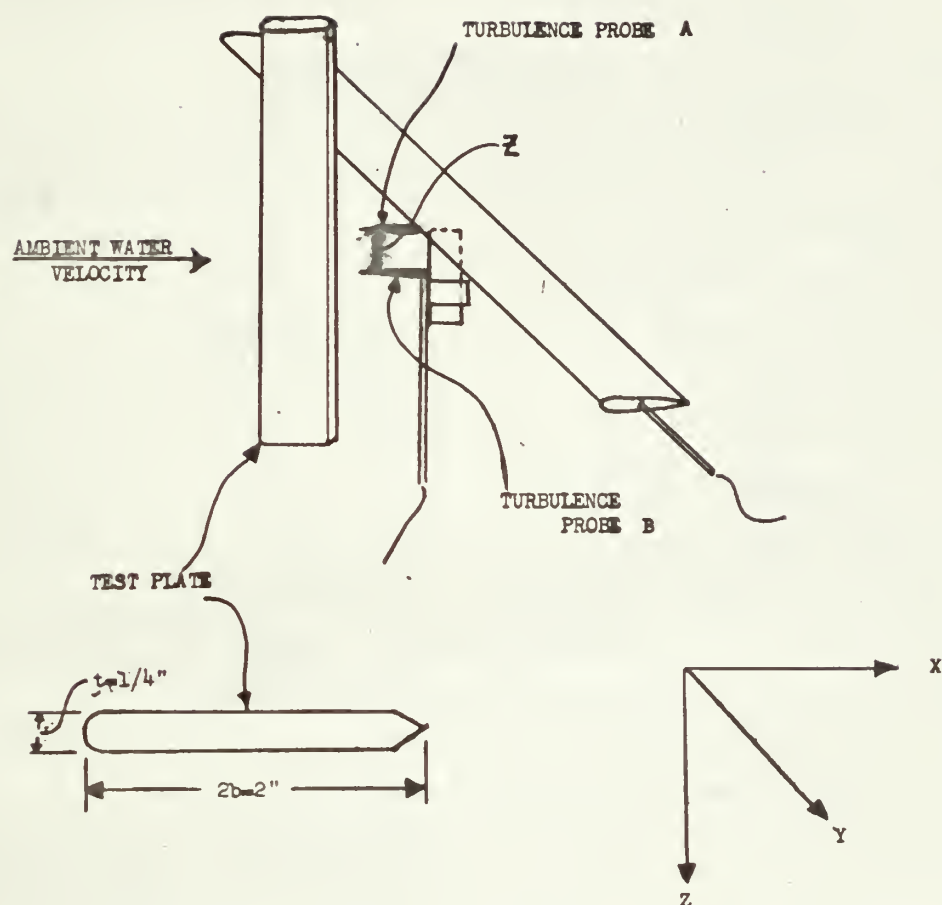
The origin of the coordinate system is located at the
center of the test section at the trailing edge of the test
plate.

Figure 15: Turbulence probe arrangement, cross section
of test plate, and coordinate system
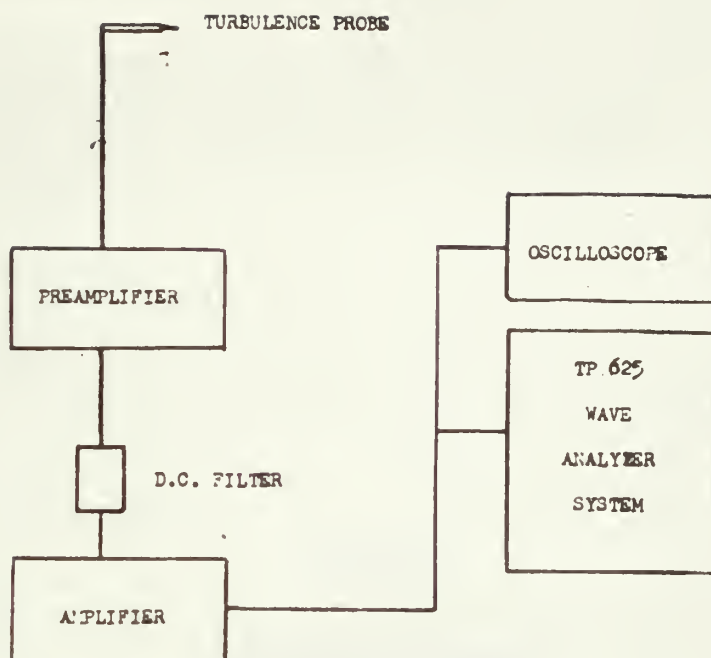
FIG.16 BLOCK DIAGRAM OF INSTRUMENTATION FOR ONE OF THE TWO
TURBULENCE PROBES

APPENDIX B

EXPERIMENTAL RESULTS
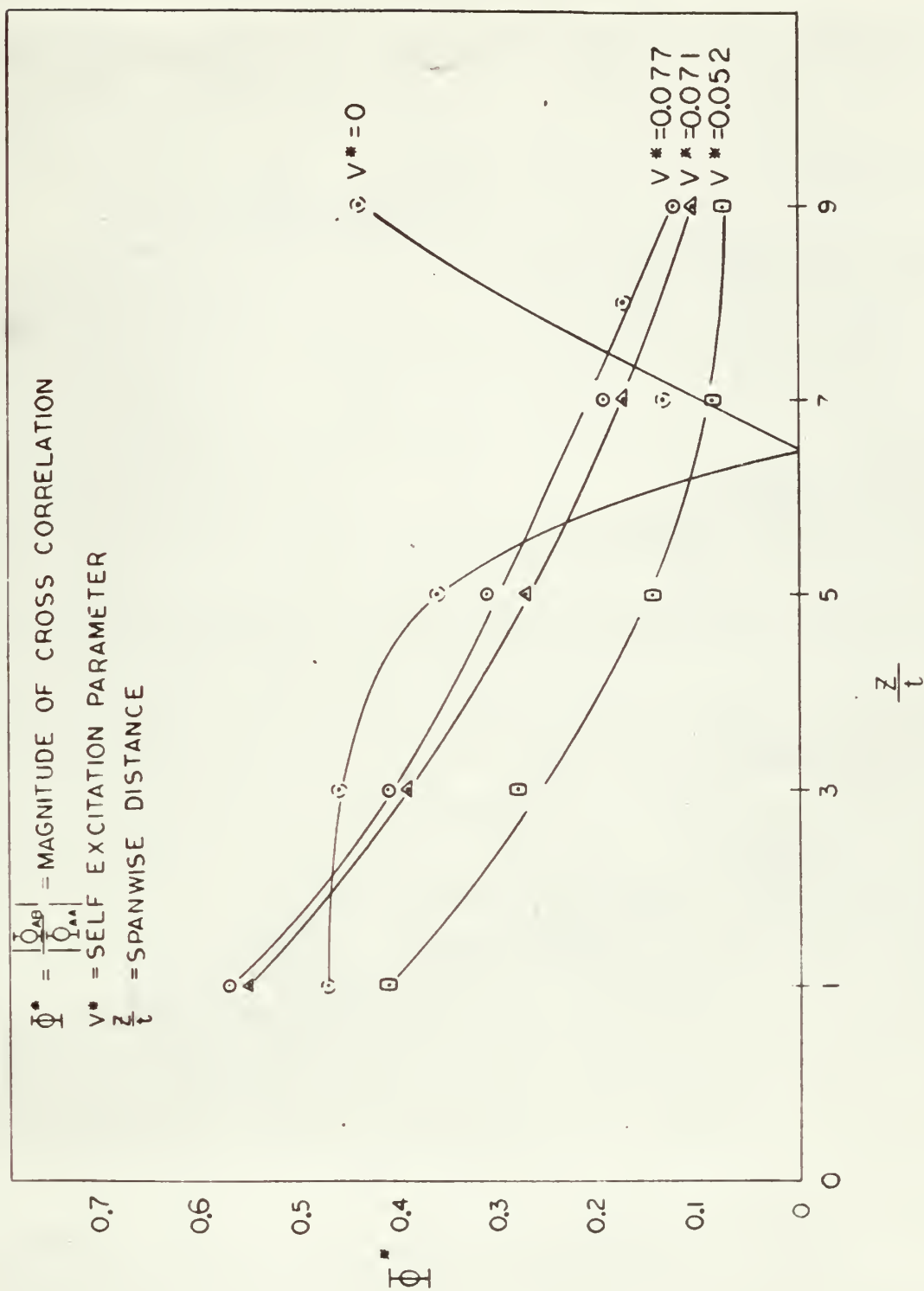
Figure 17: Normalized cross power density vs. non-dimensional spanwise distance
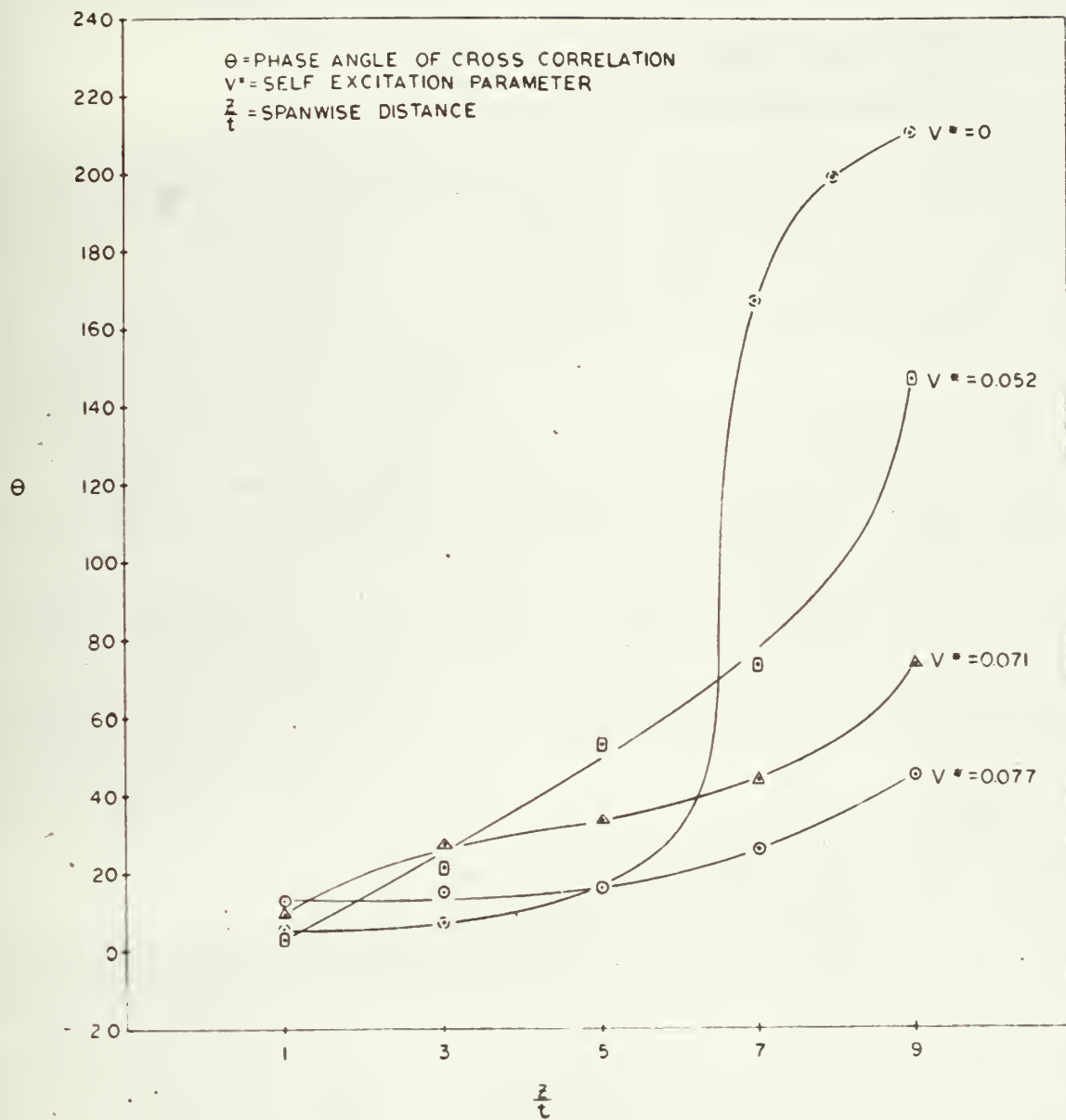
Figure 18: Correlation phase angle vs. non-dimensional spanwise distance
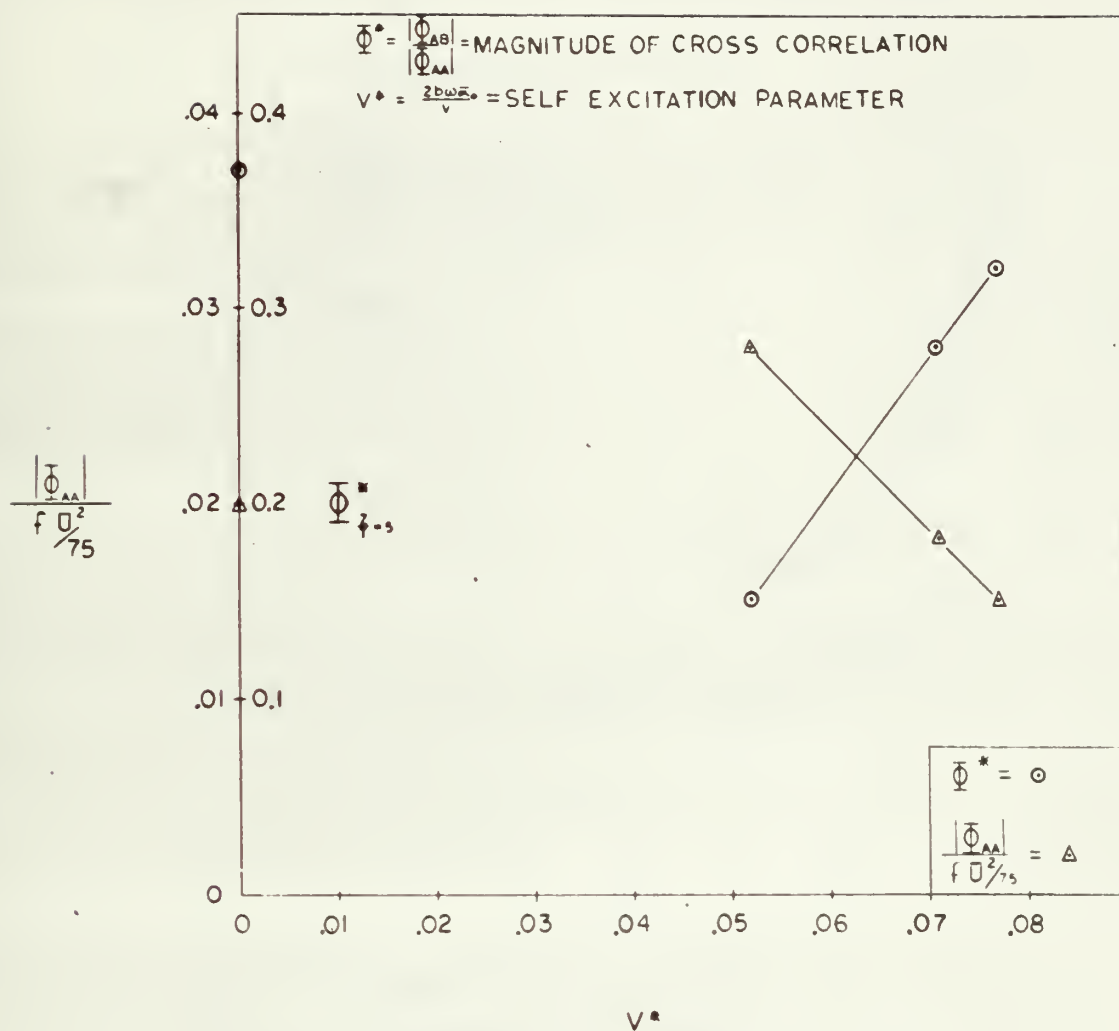
Figure 19: Normalized cross power density and vortex
strength vs. self excitation parameter
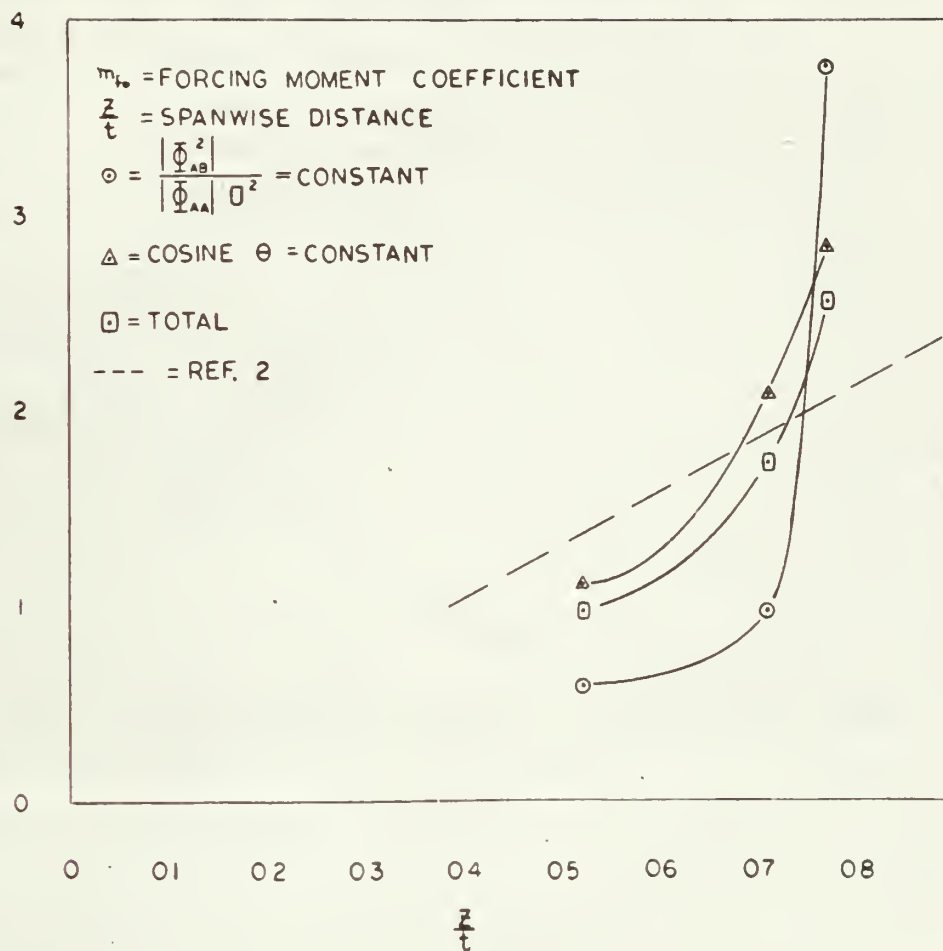
Figure 20: Forcing moment coefficient vs. self excitation
parameter
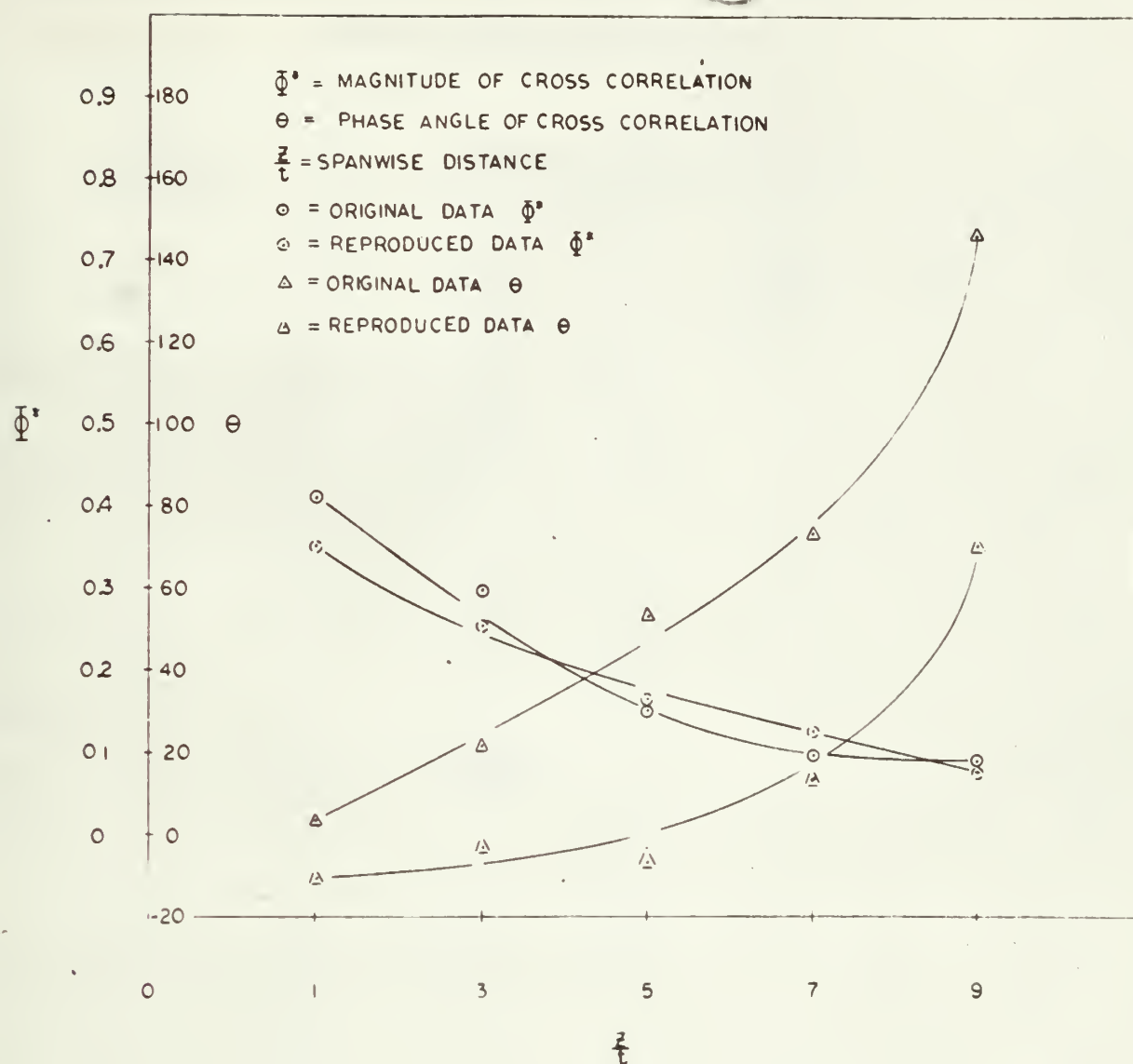
Figure 21: Reproduced results; normalized cross power density
and correlation phase angle vs. non-dimensional
spanwise distance

TABLES

Table 1 Measured Quantities

Run	z/t dimensionless distance	PSD$_A$ (volts)*	co-spectrum (volts)*	quad-spectrum (volts)*	$\overline{\alpha} \times 10^3$ (radians)	$\overline{u}$ (ft/sec)	V (ft/sec)
1	1	3.25	1.55	0.12	plate	10.85	14
2	3	"	1.50	0.20	fixed	"	"
3	5	"	1.15	0.33	$\overline{\alpha} = 0$	"	"
4	7	"	0.45	-0.10		"	"
5	8	"	-0.55	-0.17		"	"
6	9	"	-1.25	-0.73		"	"
7	1	0.55	0.31	0.07	3.93	6.04	8
8	3	"	0.22	0.06	"	"	"
9	5	"	0.17	0.05	"	"	"
10	7	"	0.10	0.05	"	"	"
11	9	"	0.05	0.05	"	"	"
12	1	1.63	0.90	0.15	4.96	9.50	11
13	3	"	0.58	0.30	"	"	"
14	5	"	0.39	0.25	"	"	"
15	7	"	0.21	0.20	"	"	"
16	9	"	0.05	0.20	"	"	"
17	1	2.0	0.83	0.00	4.63	8.50	14
18	3	"	0.53	0.21	"	"	"
19	5	"	0.18	0.24	"	"	"
20	7	"	0.05	0.17	"	"	"
21	9	"	-0.10	0.08	"	"	"

* Values measured at 105 cps for fixed plate and 75 cps for vibrating plate.

Table 2 Derived Quantities

Run	V* dimensionless velocity	Φ_{AB} (volts)	θ (degrees)	Φ^* dimensionless power spectrum	$\dfrac{\Phi^*}{\overline{u}^2}\times 10^3$	$\dfrac{\left|\Phi_{AB}^2\right|\cos\theta}{\Phi_{AA}\,\overline{u}^2}$	$\dfrac{[\Phi_{AA}]}{\overline{u}^2 f/75}$
1	plate	1.55	4.4	0.48	4.07	6.260	0.0198
2	fixed V* = 0	1.52	7.5	0.47	3.98	6.000	"
3		1.19	16.0	0.37	3.13	3.560	"
4		0.46	167.5	0.14	1.19	−0.539	"
5		0.58	198.8	0.18	1.53	−0.832	"
6		1.45	210.3	0.45	3.81	−4.770	"
7	0.077	0.32	12.7	0.58	15.90	4.950	0.0150
8	"	0.23	15.3	0.42	11.50	2.570	"
9	"	0.18	16.4	0.32	8.80	1.550	"
10	"	0.11	26.0	0.20	5.50	0.546	"
11	"	0.07	45.0	0.13	3.57	0.173	"
12	0.071	0.91	9.5	0.56	6.23	5.560	0.0181
13.	"	0.65	27.4	0.40	4.45	2.570	"
14	"	0.46	32.7	0.28	3.11	1.220	"
15	"	0.29	43.6	0.18	2.00	0.417	"
16	"	0.19	73.2	0.11	1.44	0.077	"
17	0.052	0.83	3.6	0.42	5.83	4.780	0.0278
18	"	0.57	21.7	0.29	4.02	2.100	"
19	"	0.30	53.0	0.15	2.09	0.375	"
20	"	0.18	73.6	0.09	1.25	0.063	"
21	"	0.14	146.3	0.08	1.11	−0.113	"

APPENDIX C

POWER DENSITY SPECTRA

SPECTRUM RUN 2
VEL. ⊔ Z/T 3
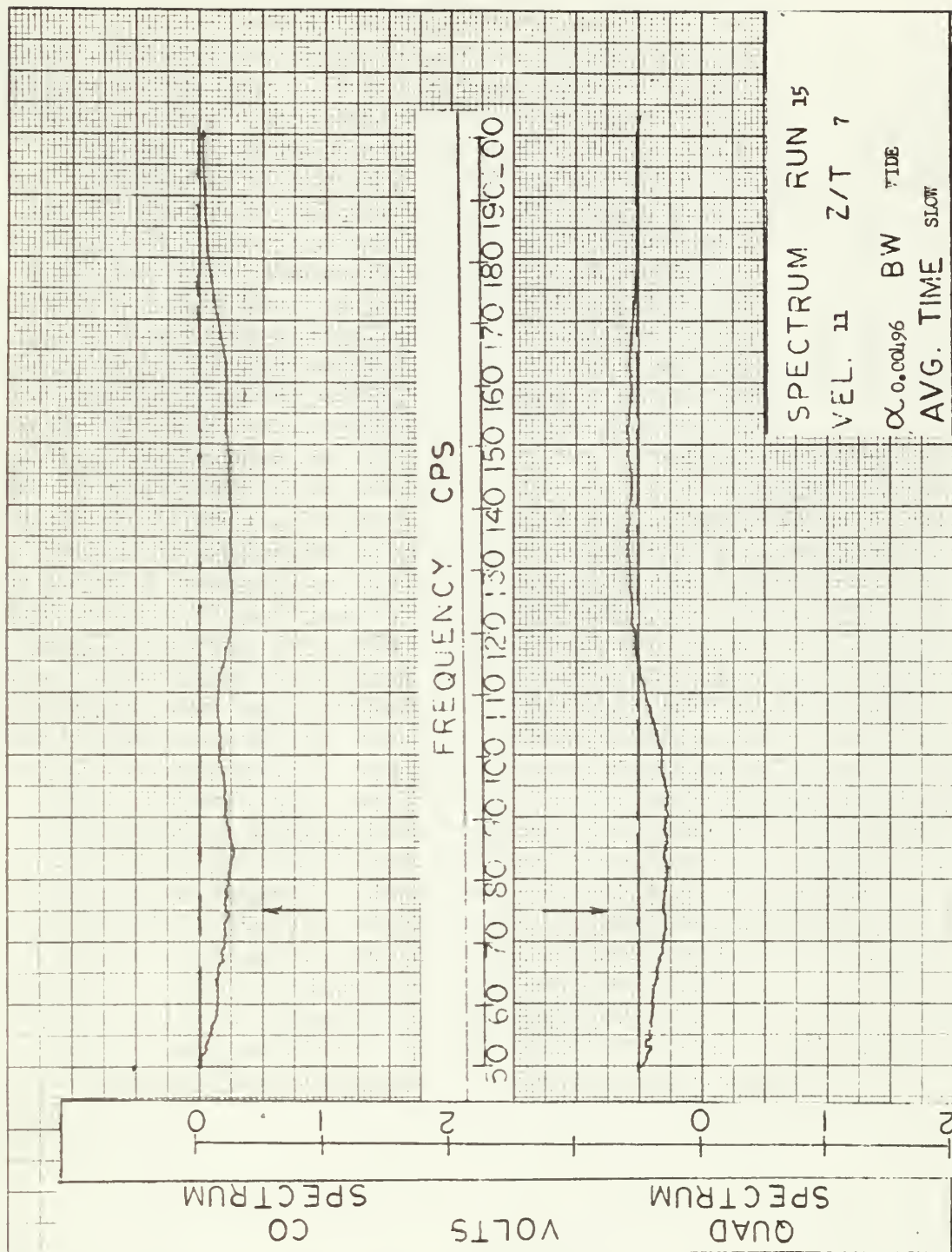α 0.0 BW WIDE
AVG. TIME SLOW

FREQUENCY CPS

VOLTS

PSD B RUN 5
VEL. ⊥ Z/T 8
∝ 0.0 BW WIDE
AVG TIME SLOW

SPECTRUM RUN 5
VEL. ⅒ Z/T 8
α 0.0 BW WIDE
AVG. TIME SLOW

FREQUENCY CPS

50 60 70 80 90 100 110 120 130 140 150 160 170 180 190 200

VOLTS

CO SPECTRUM

QUAD SPECTRUM

0 1 2

0 1 2

FREQUENCY CPS

50 60 70 80 90 100 110 120 130 140 150 160 170 180 190 200

VOLTS

0 2 3 4 5 6

PSD PLATE RUN6

VEL. 11 Z/T 9

∝ 0.0 BW NARROW

AVG TIME FAST

FREQUENCY CPS

VOLTS

PSD B   RUN 9
VEL. 8   Z/T 5
α 0.00393   BW WIDE
AVG TIME SLOW

SPECTRUM RUN 9

VEL. 8   Z/T 5

α 0.00393 BW WIDE

AVG. TIME SLOW

FREQUENCY CPS

VOLTS

PSD B   RUN 10
VEL. 8   Z/T 7
∝ 0.00393   BW WIDE
AVG TIME SLOW

SPECTRUM RUN 10

VEL. 8   Z/T 7

α 0.00393   BW WIDE

AVG. TIME SLOW

FREQUENCY CP's

FREQUENCY CPS

VOLTS

PSD ▲ RUN 11
VEL. 8 Z/T 9
∝0.00393 BW FILE.
AVG TIME SLOW

FREQUENCY CPS

50 60 70 80 90 100 110 120 130 140 150 160 170 180 190 200

VOLTS

0 1 2 3 4 5 6

PSD PLATE RUN 11
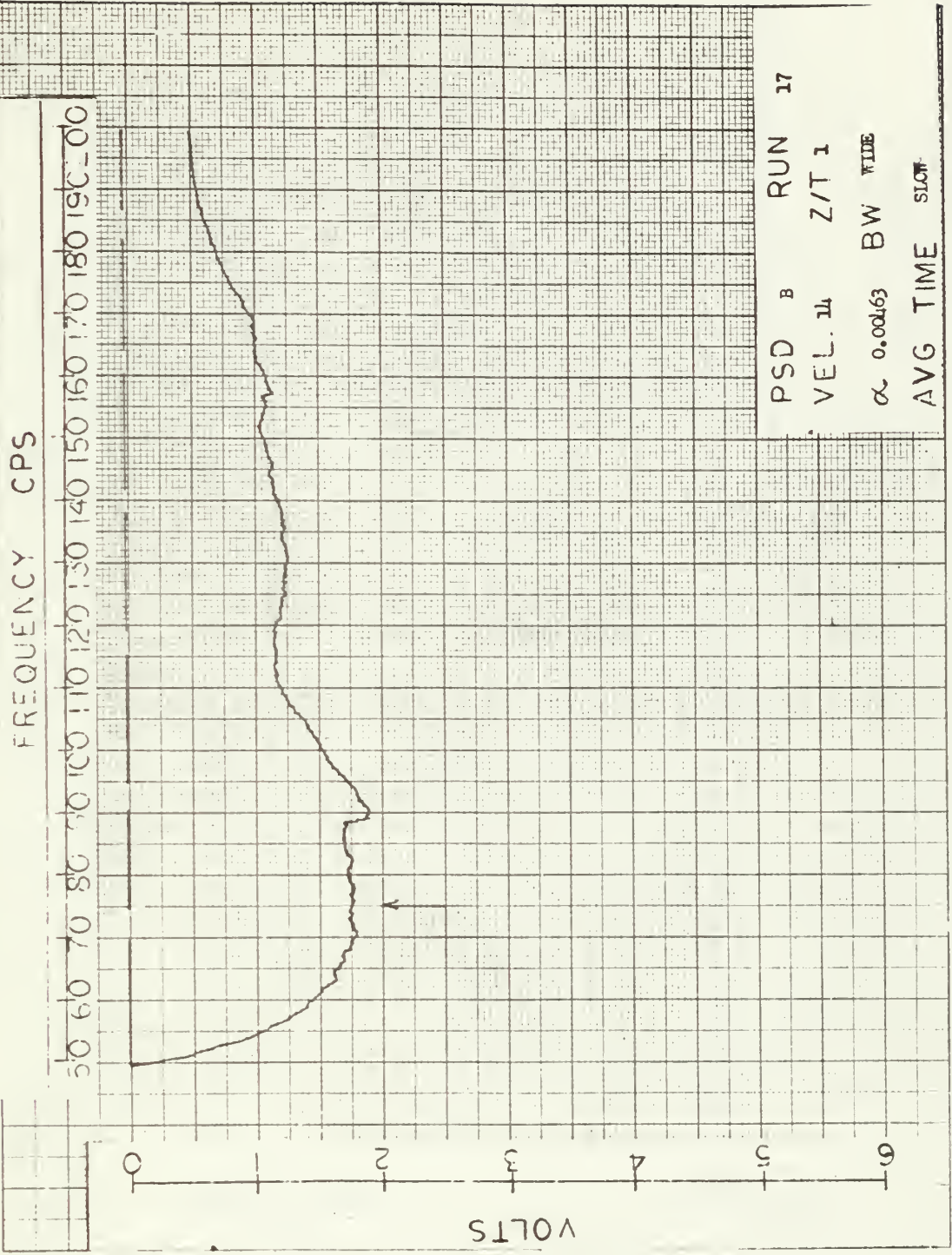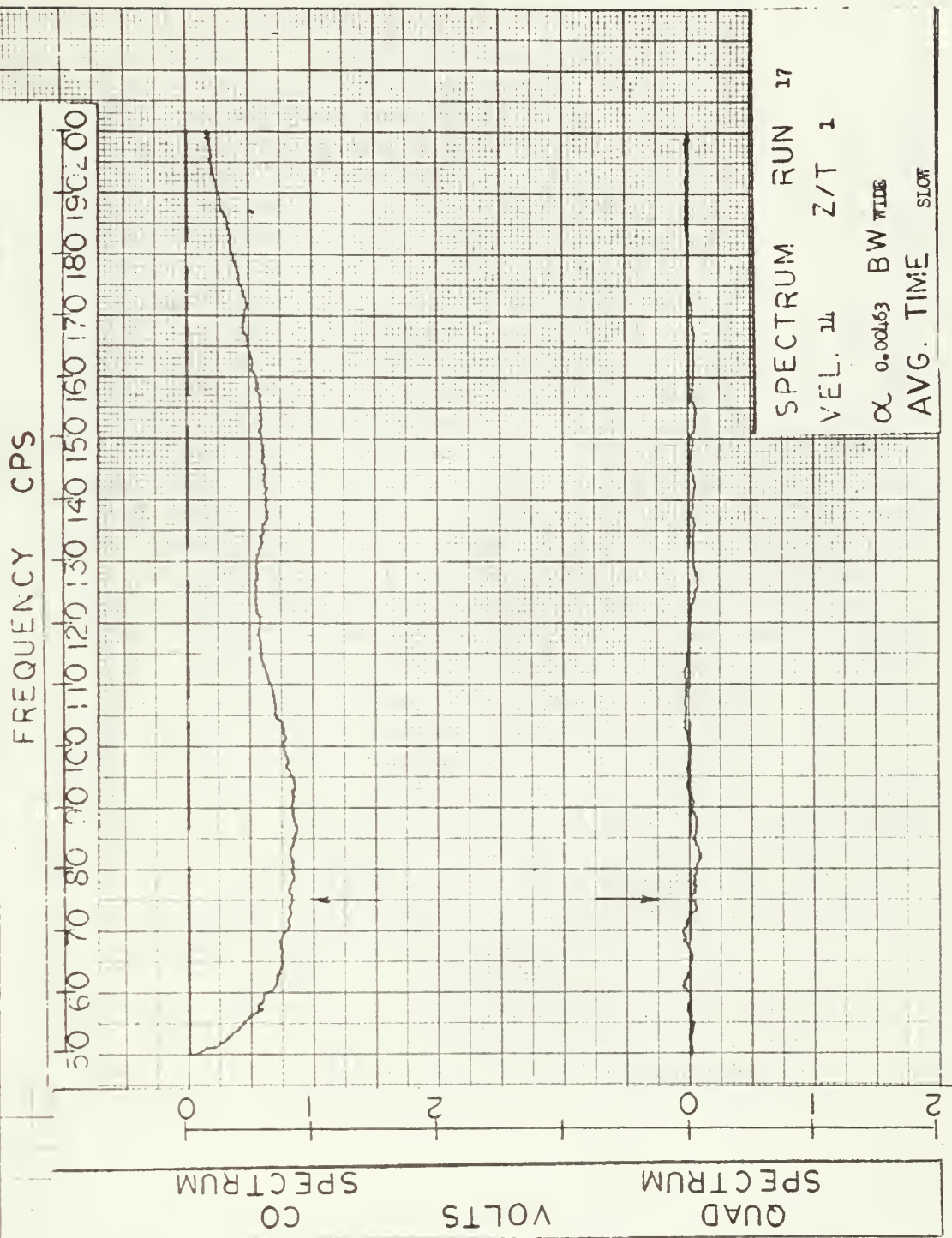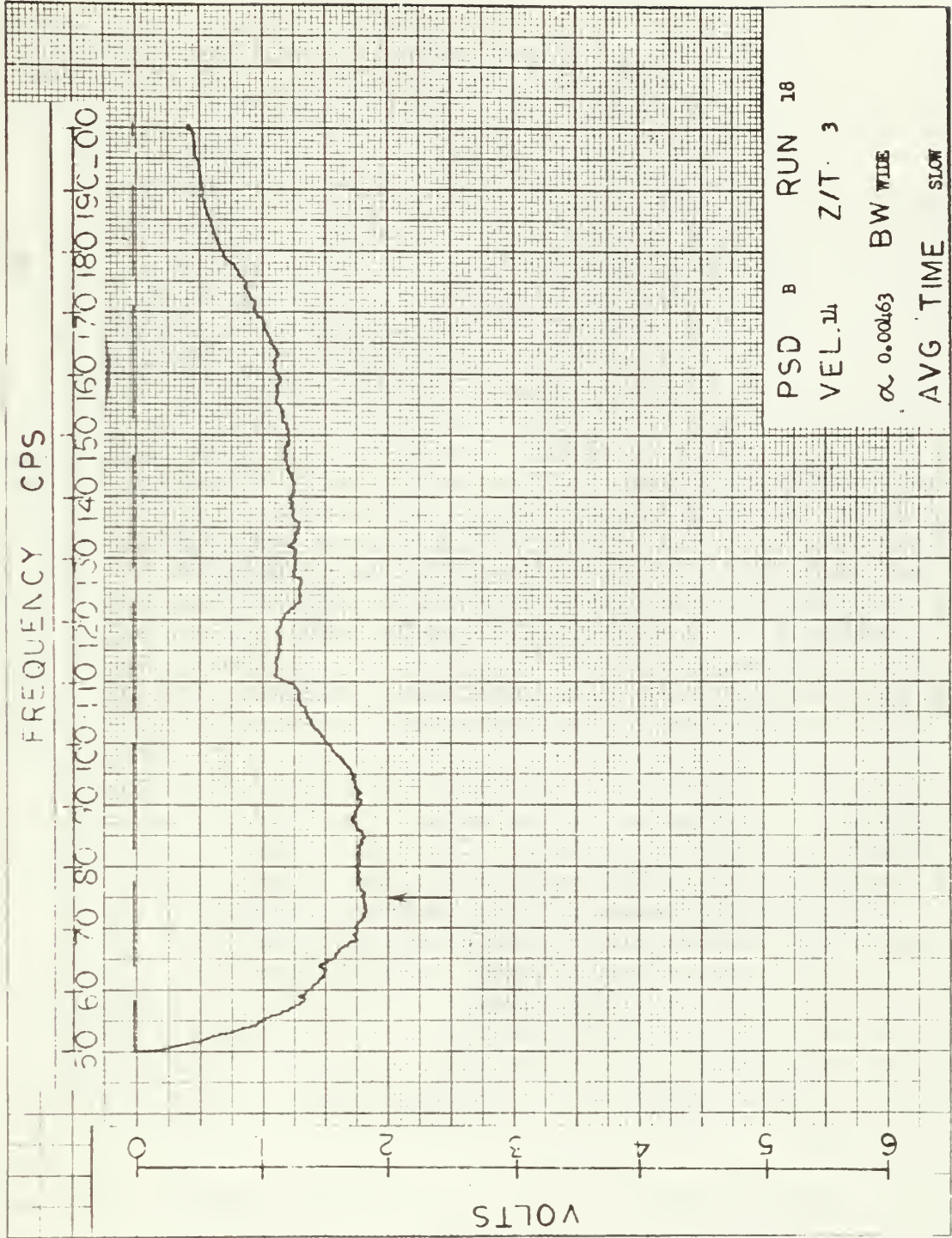VEL. 8 Z/T 9
∝ 0.00393 BW NARROW
AVG TIME FAST

SPECTRUM RUN 11

VEL. 8   Z/T 9

α 0.00393   BW WIDE

AVG. TIME SLOW

FREQUENCY CPS

50 60 70 80 90 100 110 120 130 140 150 160 170 180 190 200

CO SPECTRUM

QUAD SPECTRUM

VOLTS

FREQUENCY CPS

PSD ▴ RUN 12
VEL. 11 Z/T 1
∝ 0.00496 BW WIDE
AVG TIME SLOW

SPECTRUM RUN 12
VEL. 11 Z/T 1
α 0.00496 BW WIDE
AVG. TIME SLOW

FREQUENCY CPS

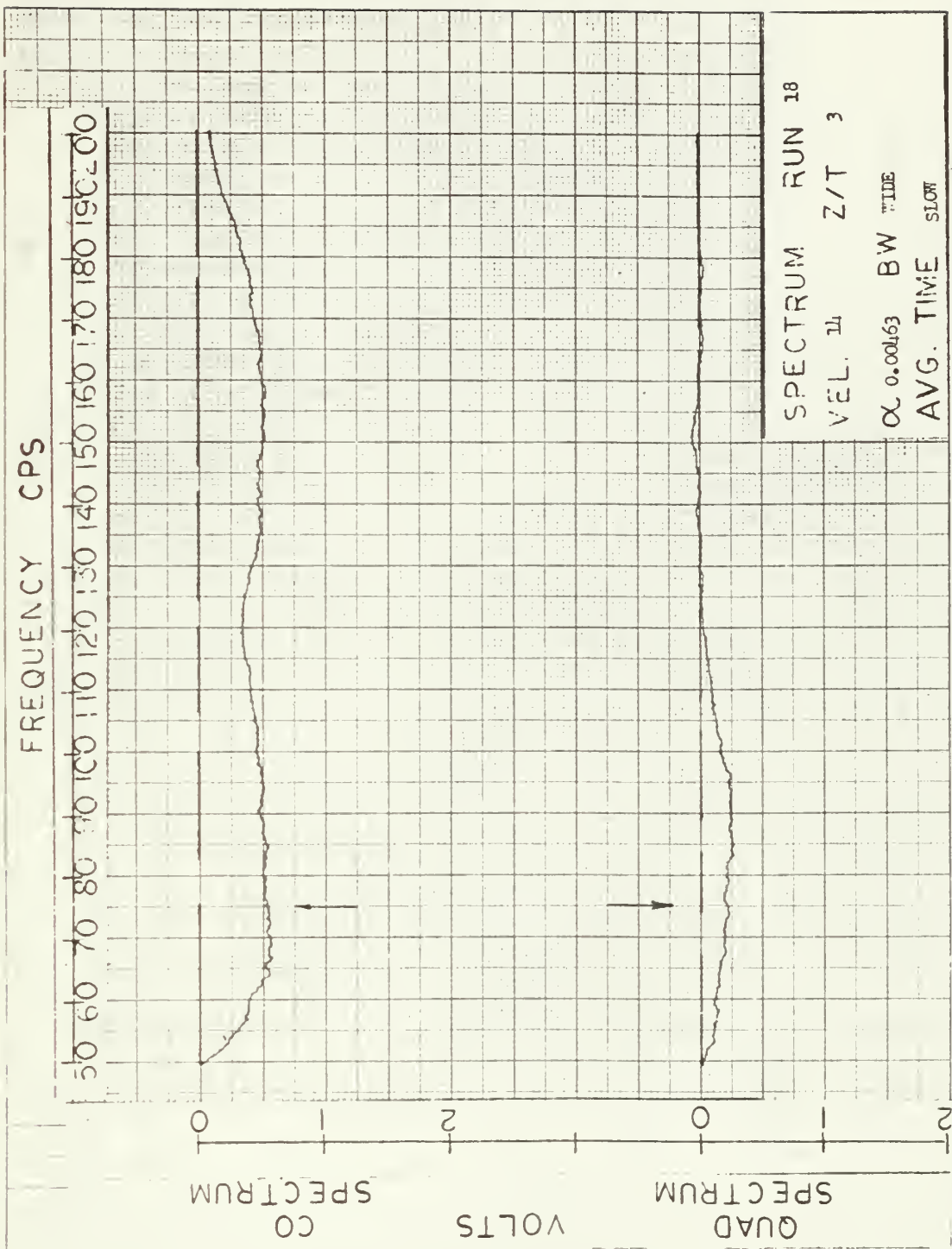50 60 70 80 90 100 110 120 130 140 150 160 170 180 190 200

CO SPECTRUM

QUAD SPECTRUM

VOLTS

FREQUENCY CPS

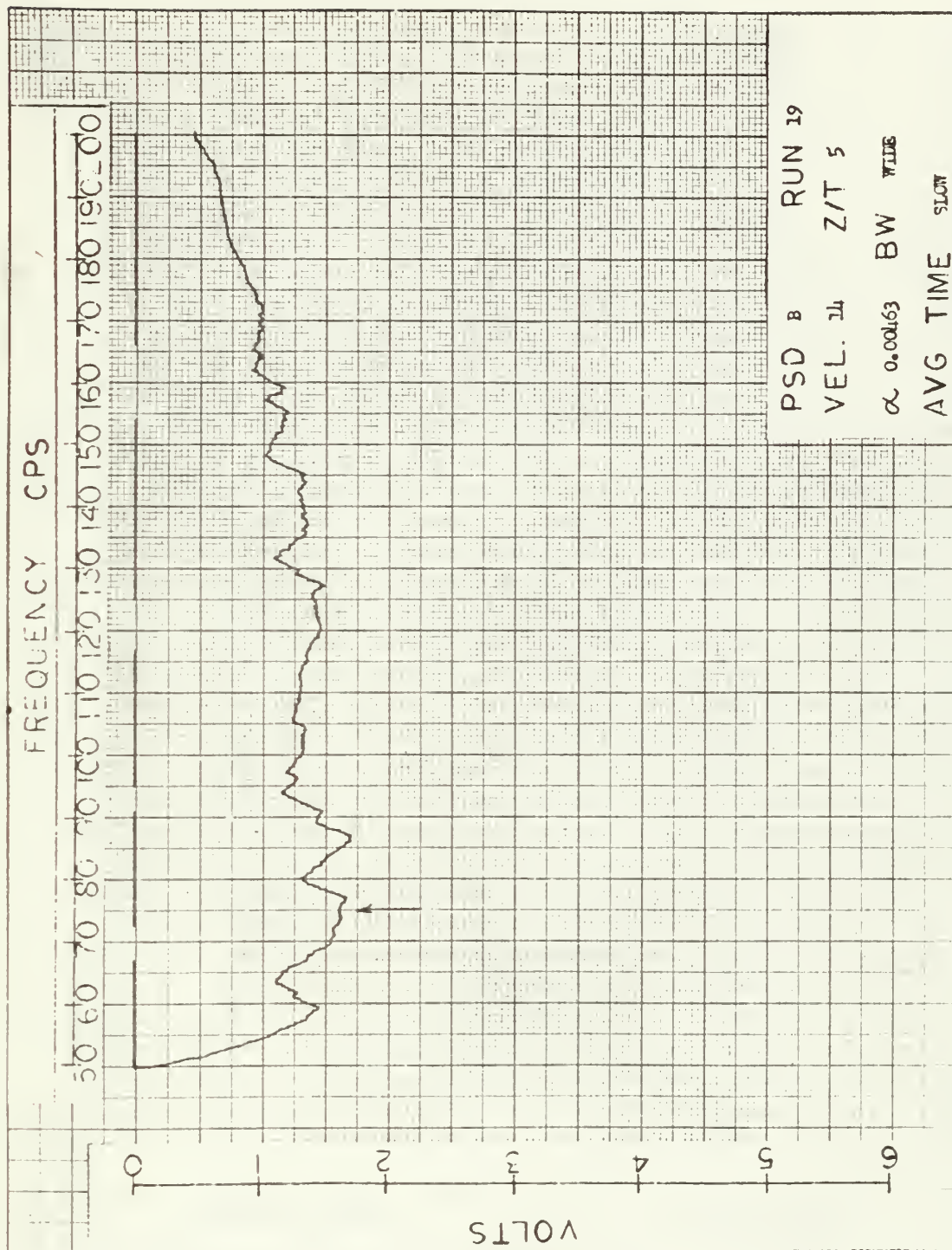PSD B   RUN 13
VEL u Z/T 3
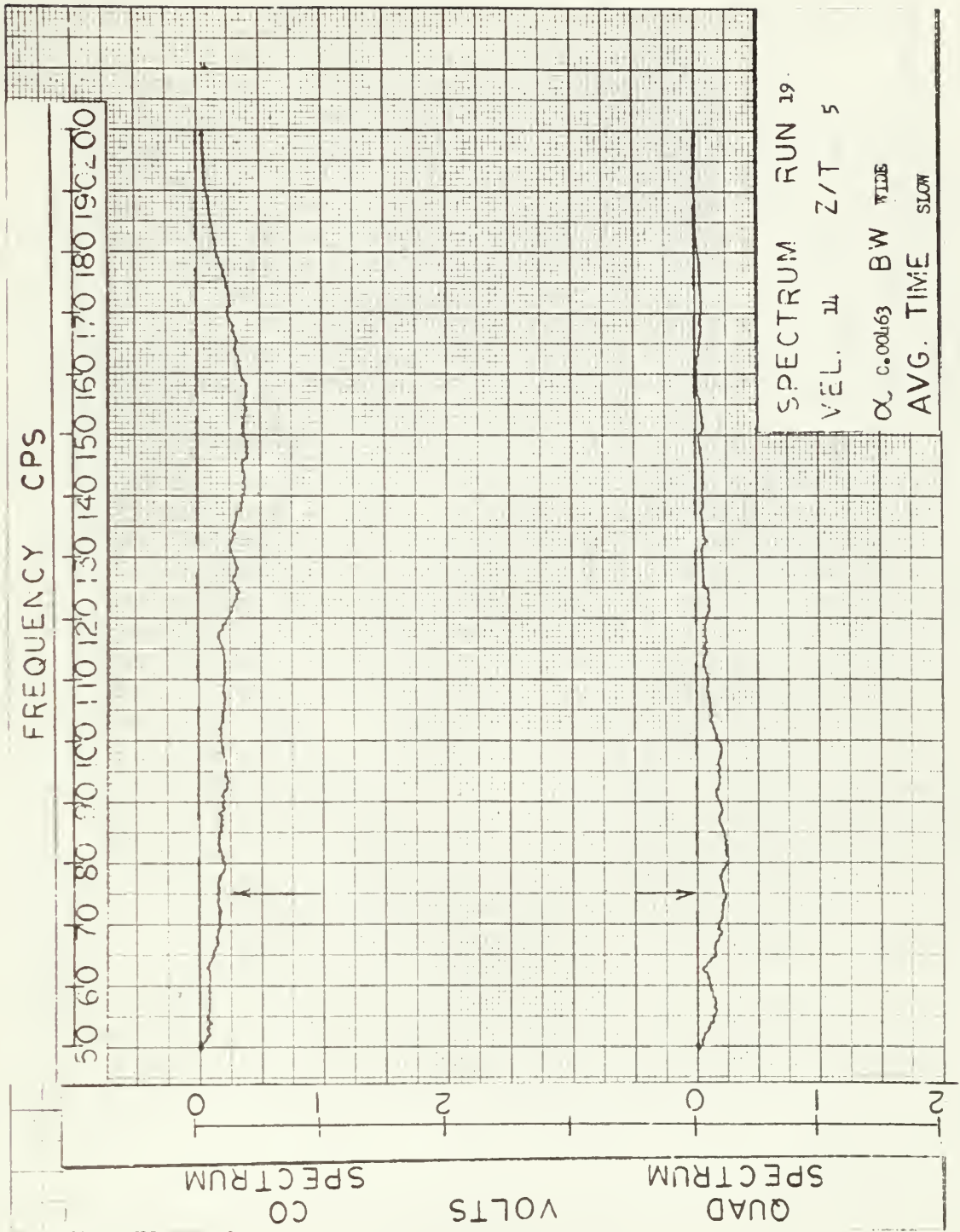∝ 0.00496 BW WIDE
AVG TIME SLOW

VOLTS

SPECTRUM RUN 13

VEL. 11   Z/T   3

α 0.00496   B W   WIDE

AVG. TIME   SLOW

FREQUENCY CPS

50 60 70 80 90 100 110 120 130 140 150 160 170 180 190 200

CO SPECTRUM

QUAD SPECTRUM

VOLTS

FREQUENCY CPS

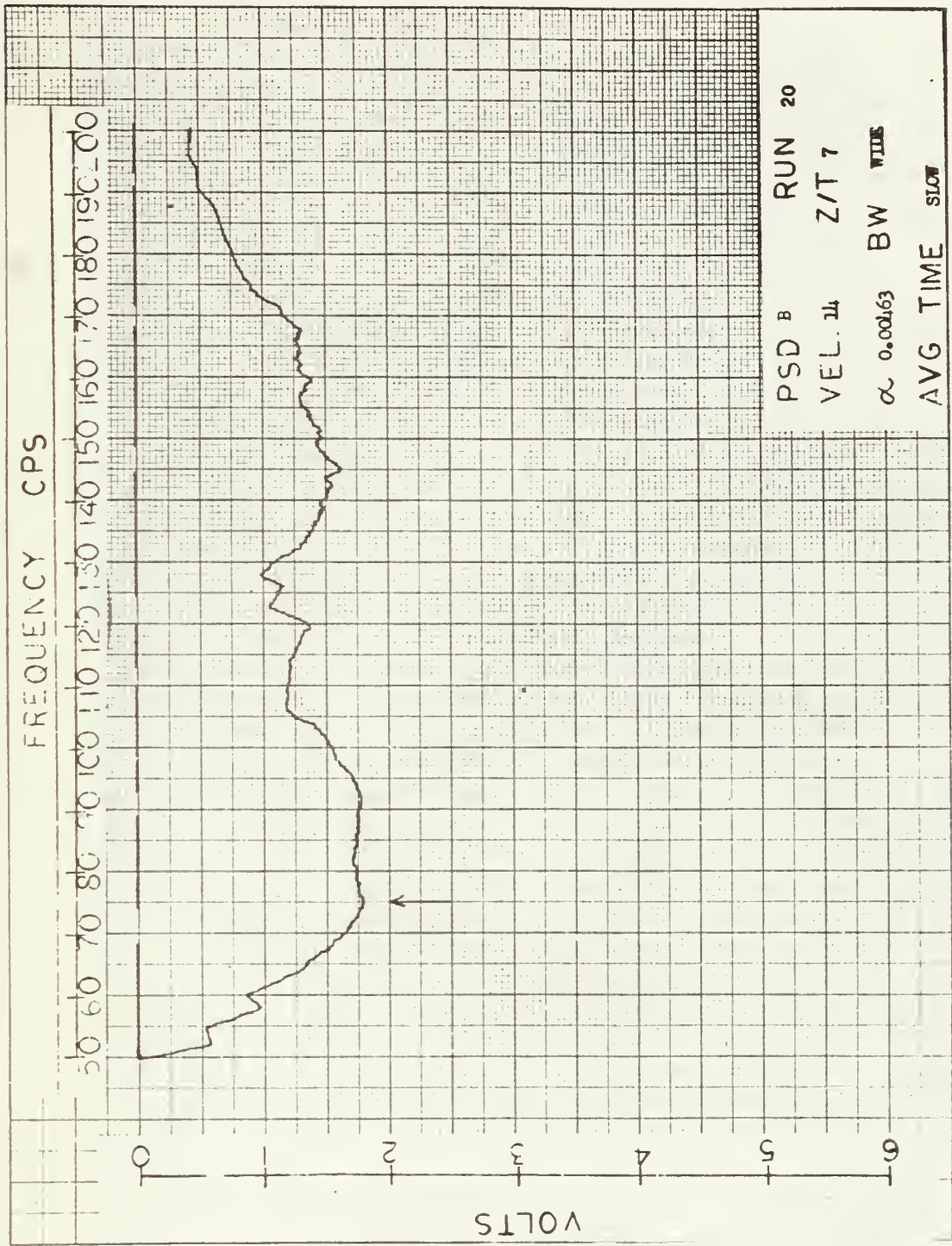50 60 70 80 90 100 110 120 130 140 150 160 170 180 190 200

VOLTS

0
1
2
3
4
5
6

PSD ᴮ   RUN 15
VEL. 11   Z/T 7
α 0.00496   BW WIDE
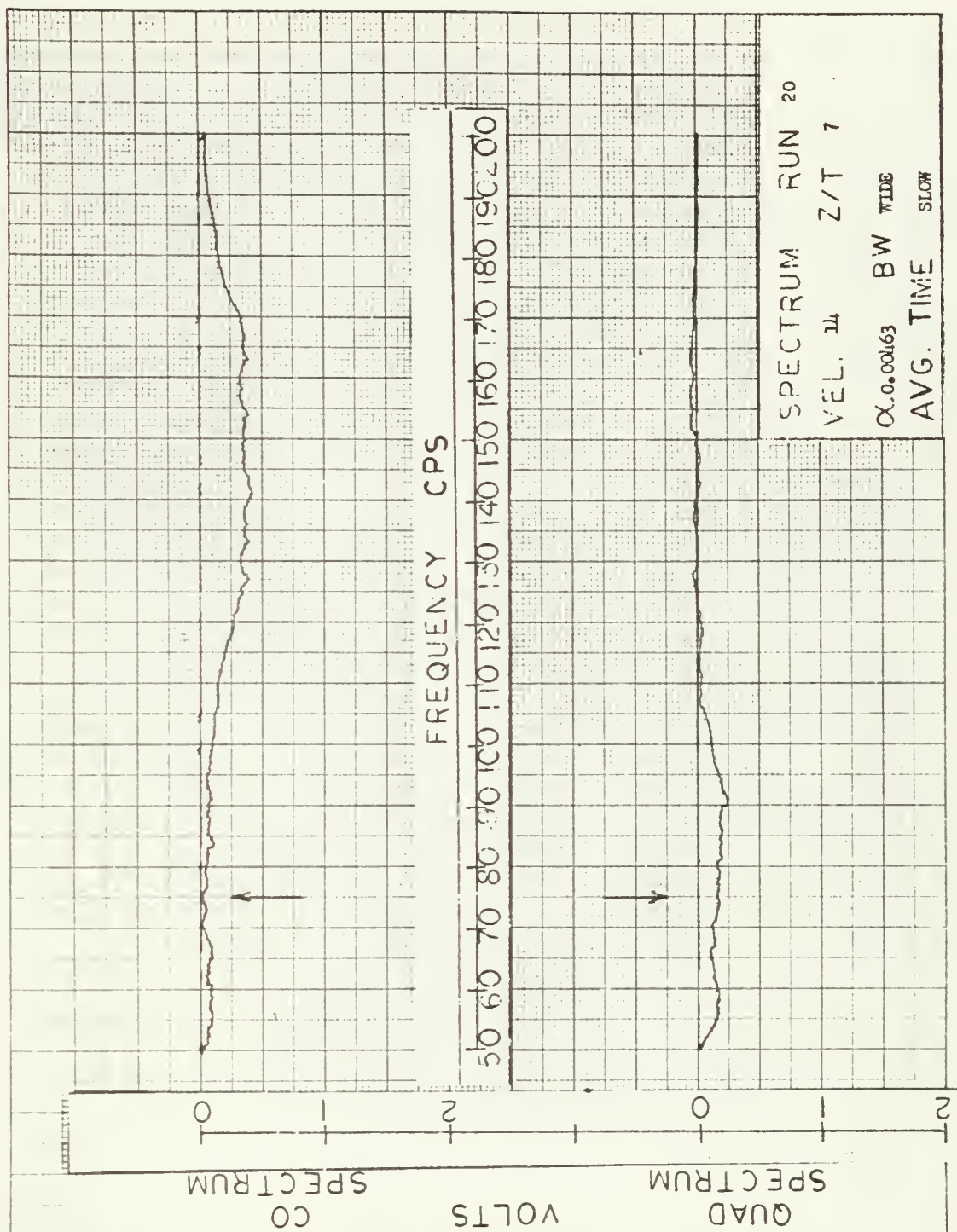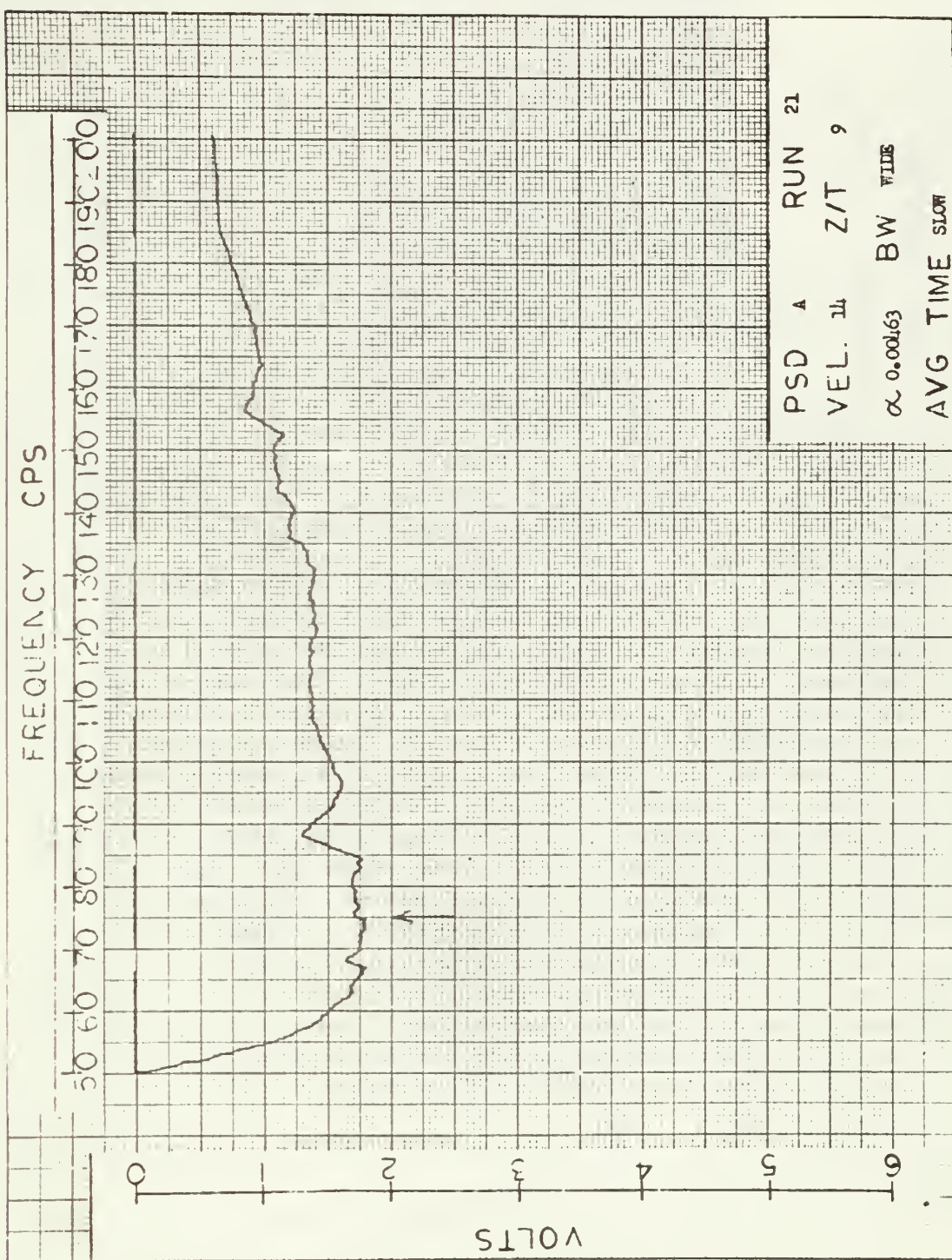AVG TIME SLOW

SPECTRUM RUN 15
VEL. 11 Z/T 7
α 0.0096 BW TIDE
AVG. TIME SLOW

FREQUENCY CPS

50 60 70 80 90 100 110 120 130 140 150 160 170 180 190 200

CO SPECTRUM
QUAD SPECTRUM
VOLTS

FREQUENCY CPS

VOLTS

PSD B RUN 16
VEL 11 Z/T 9
α 0.00496 BW NARROW
AVG TIME FAST

SPECTRUM RUN 16

VEL. 11   Z/T 9

α 0.00496   BW   WIDE

AVG. TIME   SLOW

FREQUENCY CPS

50 60 70 80 90 100 110 120 130 140 150 160 170 180 190 200

CO SPECTRUM

QUAD SPECTRUM

VOLTS

SPECTRUM RUN 19

VEL. ⊥ Z/T 5
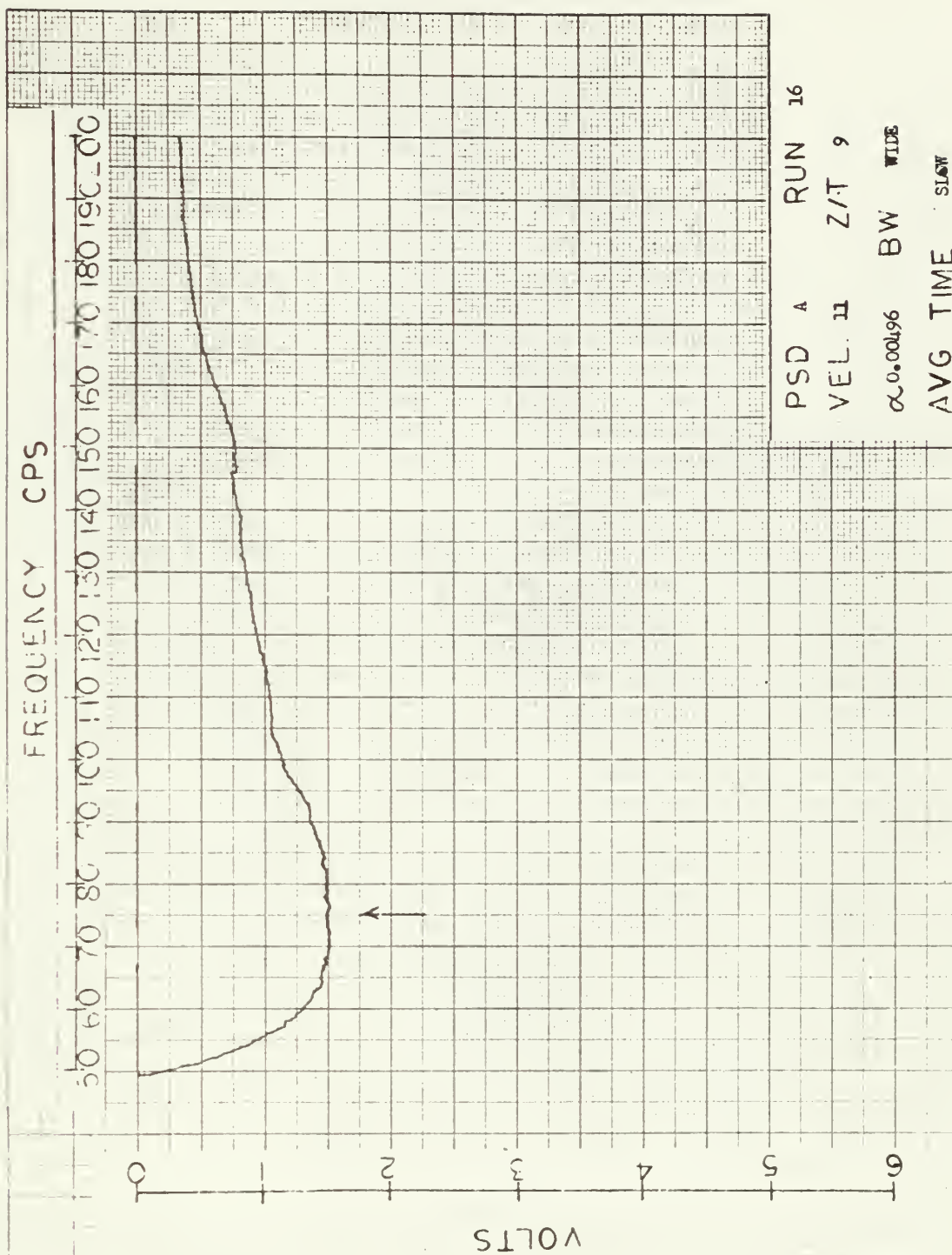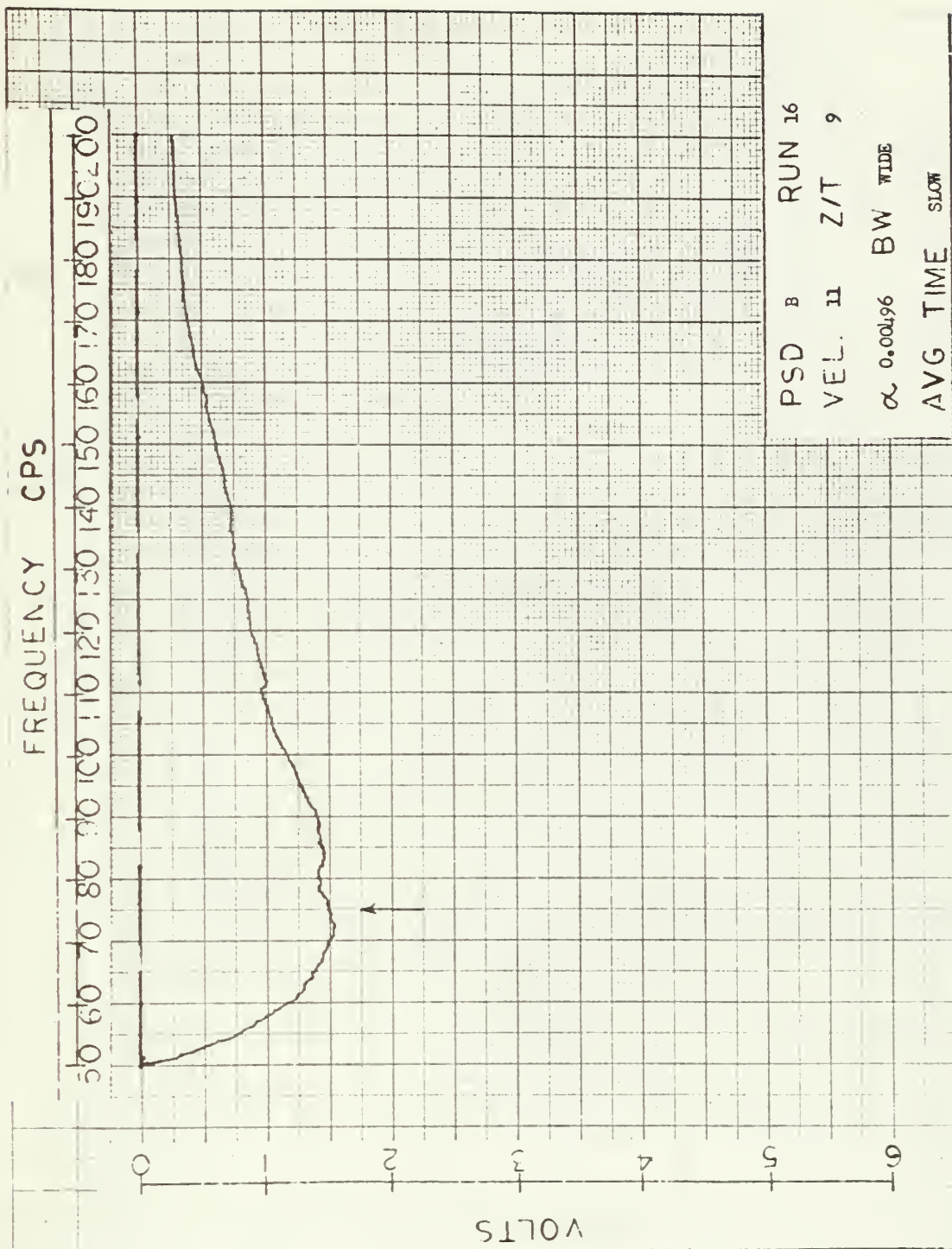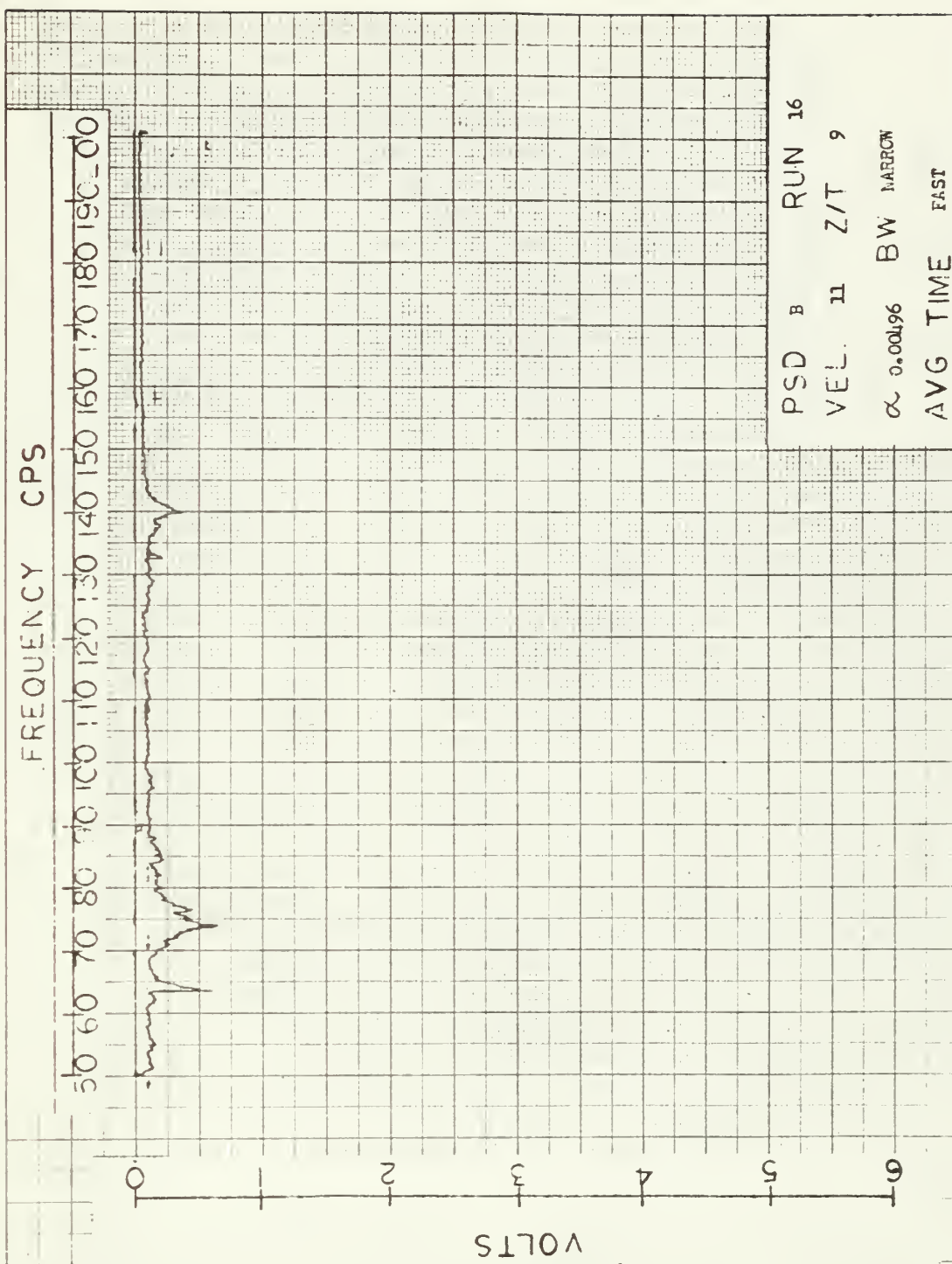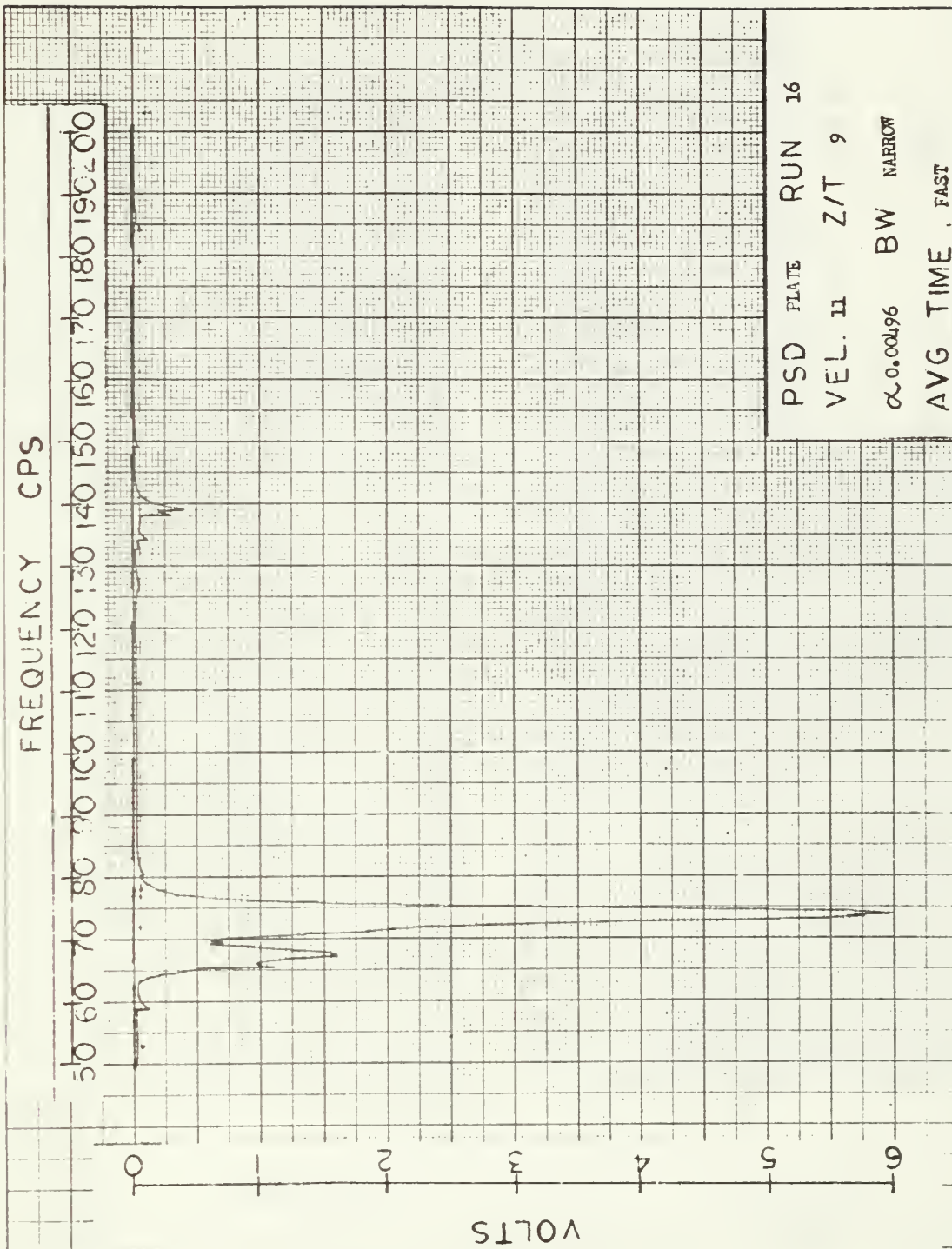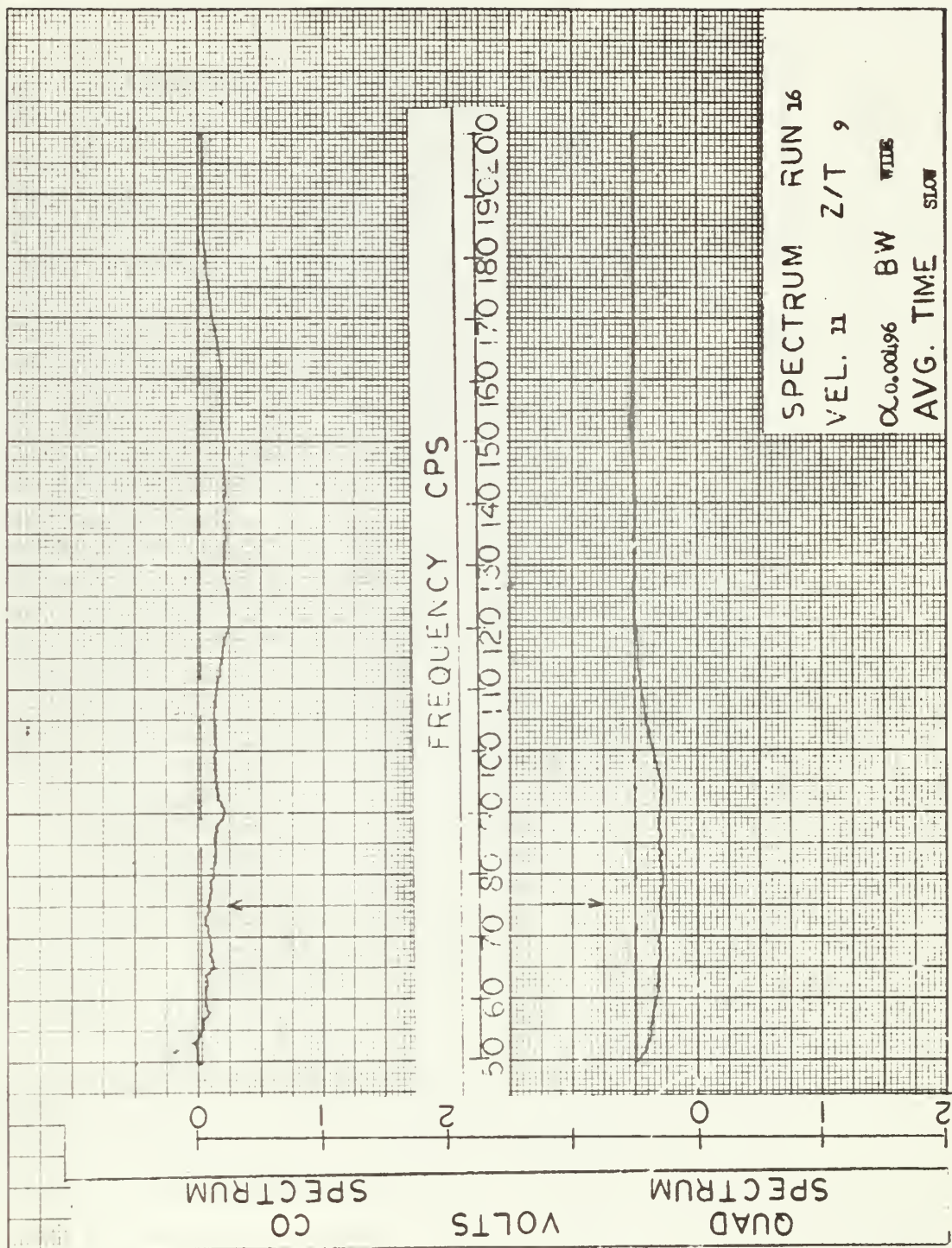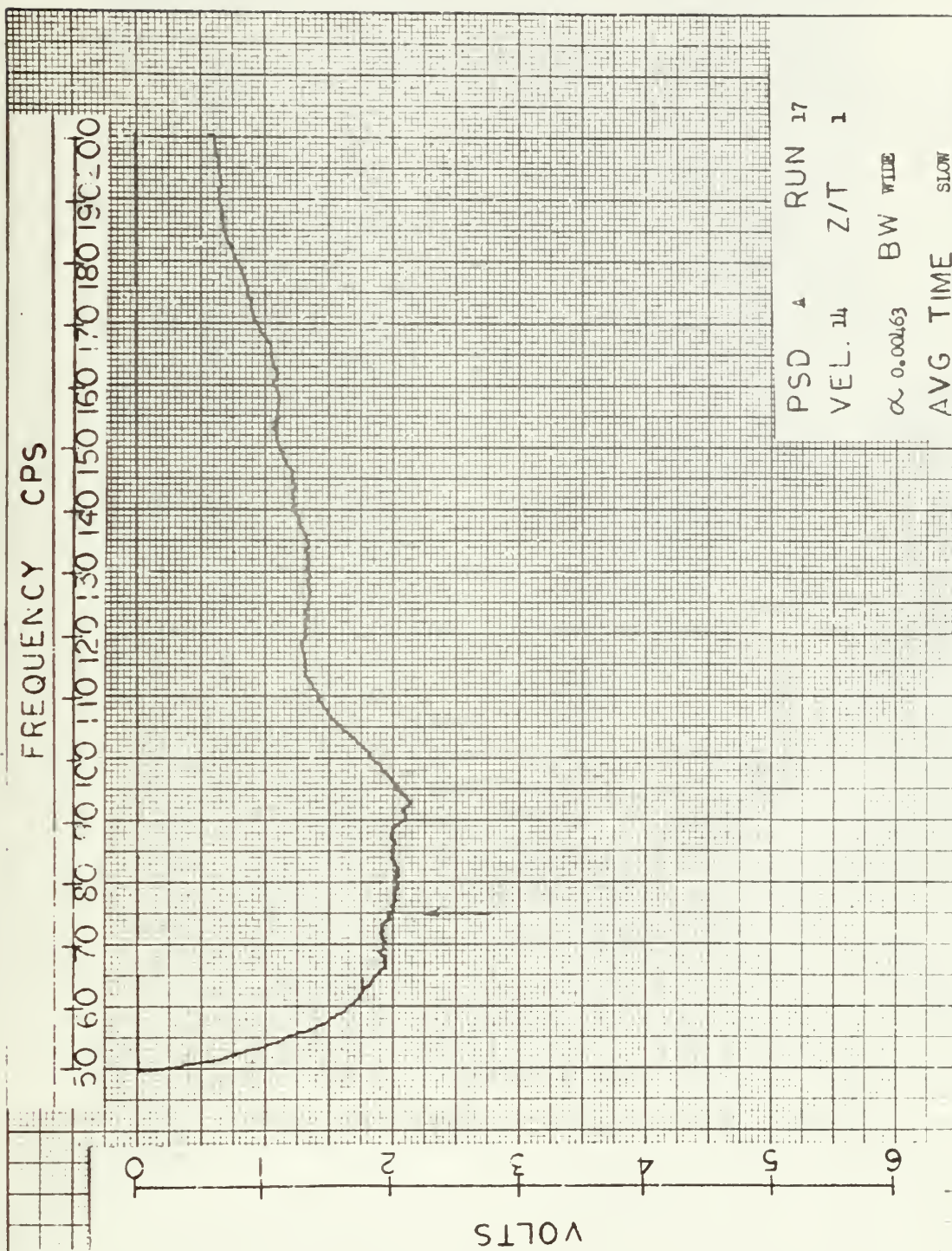
α 0.00163 BW WIDE

AVG. TIME SLOW

SPECTRUM RUN 20

VEL. u Z/T 7

α.0.0063   BW WIDE

AVG. TIME SLOW

FREQUENCY CPS

50 60 70 80 90 100 110 120 130 140 150 160 170 180 190 200

CO SPECTRUM

QUAD SPECTRUM
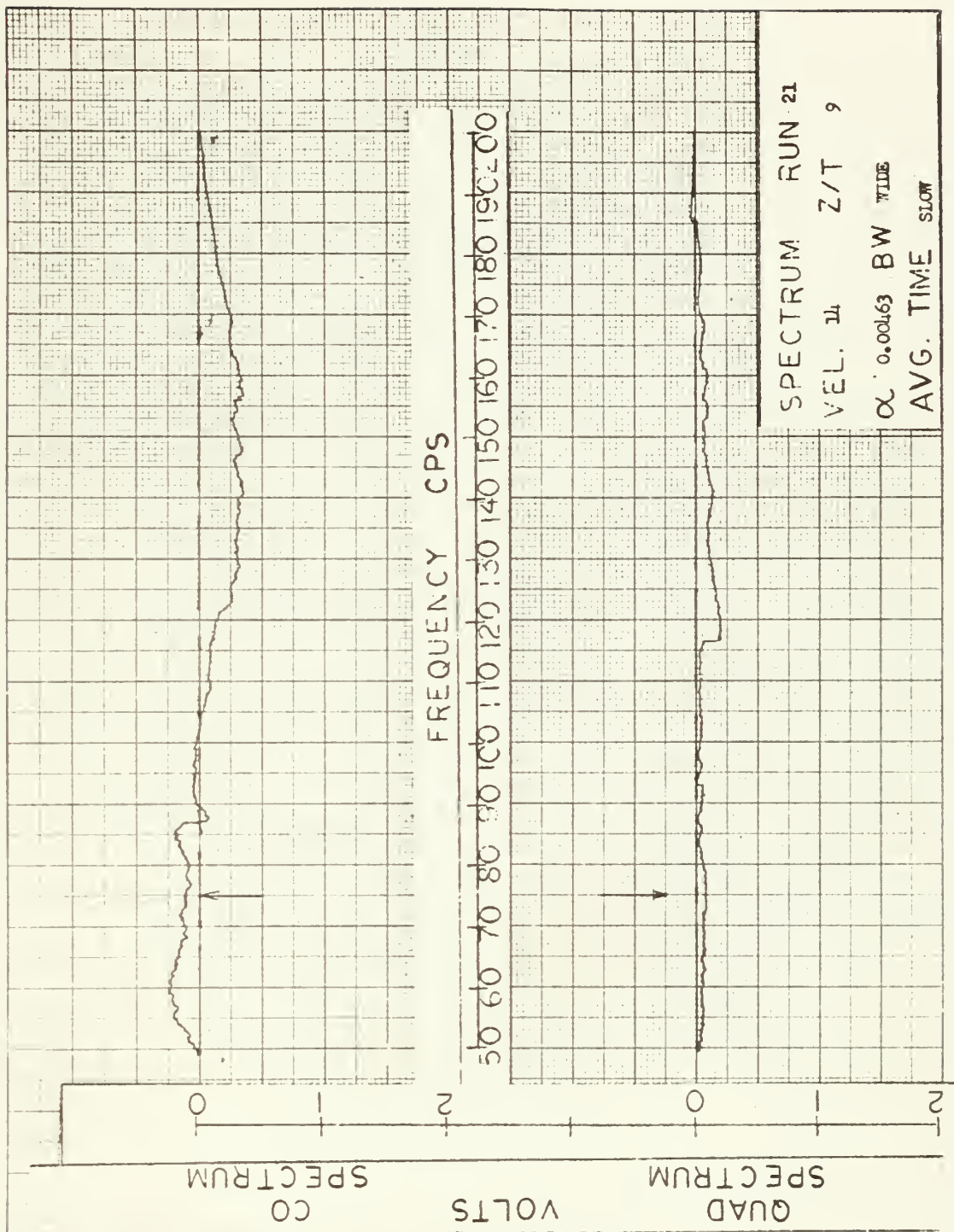
VOLTS

0   1   2

0   1   2

PSD B RUN 21

VEL Ⅲ Z/T 9

α 0.00463 BW NARROW
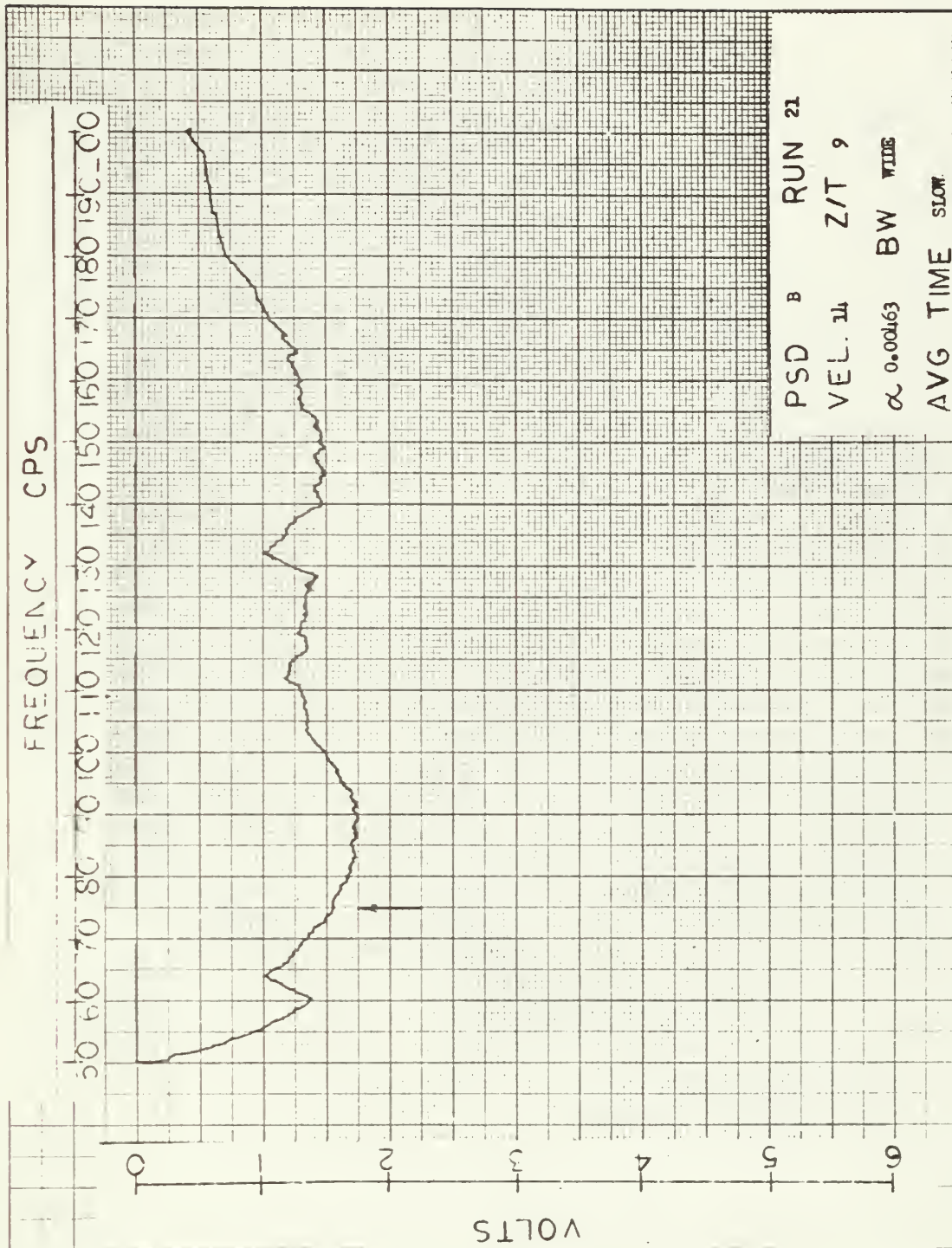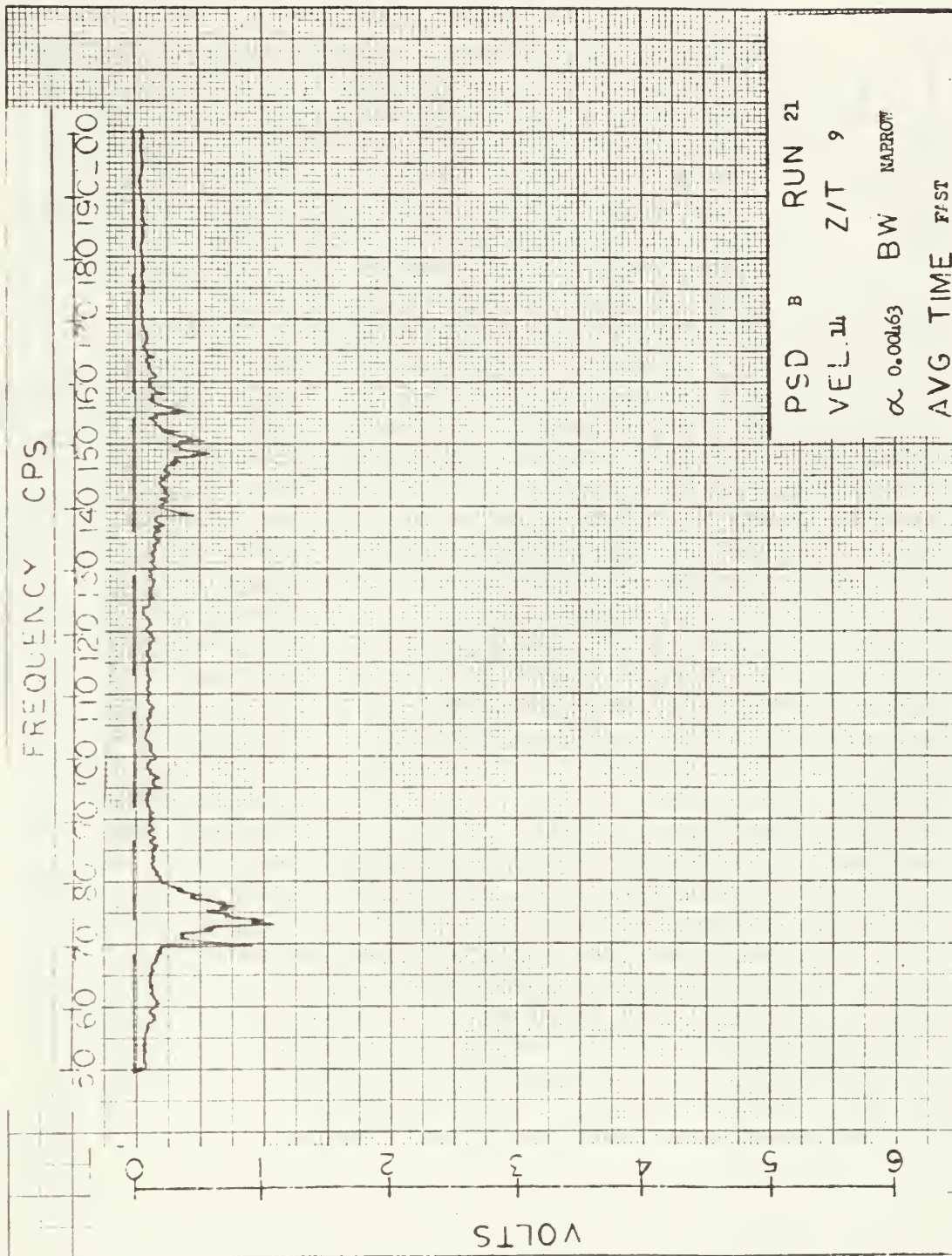
AVG TIME FAST

FREQUENCY CPS

VOLTS

FREQUENCY CPS

VOLTS

PSD PLATE RUN 21

VEL. 14 Z/T 9

∝ 0.00463 BW NARROW

AVG TIME FAST

SPECTRUM RUN 21

VEL. u Z/T 9

α 0.00463 BW WIDE

AVG. TIME SLOW

FREQUENCY CPS

50 60 70 80 90 100 110 120 130 140 150 160 170 180 190 200

CO SPECTRUM

QUAD SPECTRUM

VOLTS